A novel model for investigating the thermal equilibrium characteristics of a high-speed train gearbox

Citation for the original published paper (version of record):
Shao, S., Zhang, K., Yao, Y. et al (2025). A novel model for investigating the thermal equilibrium characteristics of a high-speed train
gearbox. AEJ - Alexandria Engineering Journal, 124: 319-336.
http://dx.doi.org/10.1016/j.aej.2025.03.100

Alexandria Engineering Journal 124 (2025) 319–336

Contents lists available at ScienceDirect

Alexandria Engineering Journal

journal homepage: www.elsevier.com/locate/aej

Original article

A novel model for investigating the thermal equilibrium characteristics of a high-speed train gearbox

Shuai Shao [a,b], Kailin Zhang [a,*], Yuan Yao [a], Yi Liu [a], Siqin Jin [c], Zhengyang Wang [d]

[a] State Key Laboratory of Rail Transit Vehicle System, Southwest Jiaotong University, Chengdu 610031, China
[b] Department of Mechanics and Maritime Sciences, Chalmers University of Technology, Gothenburg 41296, Sweden
[c] Technology R&D Center, CRRC Qishuyan Institute Co., Ltd., Changzhou 213000, China
[d] Simulation Department, Suzhou shonCloud Engineering Software Co., Ltd., Suzhou 215100, China

ARTICLE INFO

Keywords:
Gearbox
Thermal equilibrium
Moving particle semi-implicit (MPS) method
Finite element model (FEM)
Thermal network model (TNM)

ABSTRACT

Accurate analysis of the thermal equilibrium characteristics of high-speed train gearboxes can aid in preventing high-temperature malfunctions and ensuring the safe and efficient operation of trains. Owing to the complex heat transfer routes and interdependencies within the gearbox, establishing a precise thermal analysis model is essential. In this work, a finite element thermal network model is proposed to predict the temperature distribution of a gearbox. The moving particle semi-implicit method is used to determine the flow state of the lubricant and the convective heat transfer coefficients on the surfaces of the components. Power loss, which contributes to heat generation, is categorized into gear meshing, oil churning, and bearing friction. A thermal network model and finite element model for thermal analysis are subsequently developed based on heat transfer relationship, and data exchange between the two models is achieved through the BoundaryToFEM unit. The effects of the gear rotation speed, convective heat transfer coefficient between the components and lubricant, and heat transfer coefficient between the outer surface of the gearbox and ambient air on the thermal equilibrium are analyzed. The results indicate that when the input gear speed increases from 2104 rpm to 5259 rpm, the total power loss increases by 2159 W, and the heat balance temperature increases by approximately 53 °C. When the convective heat transfer coefficient between the components and lubricant varies from a 50 % reduction to a 50 % magnification, the thermal equilibrium temperature only changes by 1–2 °C. However, when t between the outer surface of the gearbox and ambient air undergoes the same variation process, the thermal equilibrium temperature decreases by approximately 82 °C. The full-scale gearbox running-in experiment shows that the predicted temperatures of the bearing cups remained within a deviation range of 2–5 % from the experimental values, and the maximum error of the lubricant temperature was 3.18 °C, which further verifies the accuracy and reliability of the proposed model.

1. Introduction

The electric transmission system, known for its efficiency, stability, and controllability, is widely used in modern high-speed trains (HSTs) [1,2]. The system is composed of a traction motor, elastic coupling, gearbox, and wheelset, which guarantees precise and efficient power transmission [3]. The gearbox transmits the torque of the traction motor to the wheelset through gear meshing to drive the train. However, as the train speed increases, the working conditions of the transmission system become more complex and harsh. As a critical component, the gearbox operates in a high-temperature, high-speed and high-load environment and faces problems of heat accumulation and efficiency degradation [4,5]. These factors not only affect the reliability of the transmission system but also pose a potential threat to the safety of train operations. Therefore, studying the thermal equilibrium of a gearbox, particularly the temperature distribution and thermal management, is valuable for improving transmission efficiency, optimizing heat dissipation structure design and extending service life.

The precise calculation of power loss serves as the basis for analyzing the thermal equilibrium of the gearbox. The gearbox power loss can be divided into load-related power loss and nonload-related power loss [6]. Among them, gear meshing power loss and bearing friction power loss are functions of the load, friction coefficient, and rotational speed, whereas gear churning loss is related to factors such as the rotational

* Corresponding author.
E-mail address: zhangkailin@swjtu.cn (K. Zhang).

https://doi.org/10.1016/j.aej.2025.03.100
Received 11 April 2024; Received in revised form 12 November 2024; Accepted 24 March 2025
Available online 4 April 2025

speed and lubricant viscosity [7–11]. The current power loss calculation analyzes the working mechanisms of various friction pairs and establishes a numerical model to solve for power loss during the friction process. Based on gear contact analysis, the meshing principle and tribology theory, the influence of gear geometric parameters and working conditions on meshing power loss was discussed in [7,12–20]. Numerous calculation models are summarized on the basis of extensive experiments, such as the Anderson model [13], Coy & Townsend model [15], ISO/TR 14179 model [17,18] and Seetharaman model [20]. However, these models must adhere strictly to their application conditions; otherwise, significant errors may result. In existing studies on bearing friction power loss, the integral method and the local method are usually used. The integral methods [21–25] are based on empirical formulas, which are simple and widely used in engineering. Local methods [9,10,26,27] provide more detailed analyses of bearing components, including rollers, cone and cup assemblies, and lubricants. Although these methods offer higher accuracy, they are more complex, have a narrower application range, and are less efficient than the overall methods in engineering applications. In addition, research on oil churning loss is continuously progressing. Experimental methods are commonly used to acquire data on churning loss, and empirical formulas such as those by Terekhov [28], Boness [29], and Luke [30] have been developed. Changenet and colleagues [31–33] refined experimental techniques, thoroughly explored the factors affecting churning loss and developed more accurate predictive models. In addition, computational fluid dynamics (CFD) simulations are widely used to analyze the hydrodynamic behavior and churning loss mechanism [6,34–36]. Although CFD simulation can provide high-precision results, its calculation is very expensive and resource intensive, especially in complex systems, and the simulation time is very long.

The heat in the gearbox comes mainly from the friction between the components. If heat cannot be dissipated in time, it will lead to an increase in oil temperature, a decrease in lubrication performance and aggravation of component wear, which will ultimately affect working performance and operation stability. Consequently, heat transfer analysis and thermal management of gearboxes have become important research fields. At present, methods for analyzing the thermal characteristics of gearboxes include experimental techniques, finite element analysis and the thermal network method. Researchers have built test rigs and employed thermocouples and infrared imaging to directly measure the temperatures of bearings, gears, lubricants and casings [37–41]. Nonetheless, experimental methods incur high labor costs and face some limitations when applied under complex conditions. The finite element method has emerged as an important research technique because it can simulate the complex temperature distribution within a gearbox. Shi et al. [42] used the finite element method to simulate the tooth surface temperature distribution of a locomotive drive spur gear. Li et al. [43] investigated the effect of the helix angle on the temperature distribution of gears. Refs. [44–46] systematically analyzed the factors influencing the gear temperature field. In these studies, the large-scale flow behavior of the lubricant is decoupled from the gear motion, and an estimated convective heat transfer coefficient (HTC) is used to represent the heat dissipation behavior of the gear. Lu et al. [47,48] established a thermal—fluid coupling model of an intermediate gearbox and evaluated the correlation between the convective HTC and the tooth surface temperature. Bashal et al. [49] studied the oil flow and the temperature distribution on the rotor surface of a multinozzle screw compressor. Owing to differences in mesh types, CFD models for the flow field and temperature field must be established individually for thermal—fluid coupling analysis, and data exchange between models is achieved through specific scripting programs. In addition, finite element simulations of thermal—fluid coupling require considerable resources and time. The simulation quality is subject to the user experience, and the postprocessing process is cumbersome. The thermal network method is an alternative approach for analyzing thermal characteristics. Compared with finite element analysis, the thermal network method only needs to establish a one-dimensional thermal network model (TNM), which simplifies the solution process to the solution of linear equations. Scholars have applied the thermal network method to FZG gearbox [50], four-stage transmission [51], automobile drive axle [52], six-speed manual gearbox [53] and planetary gearbox [54] and verified the accuracy of the TNM through experiments. This shows that the thermal network method is very suitable for analyzing the thermal equilibrium characteristics of the gearbox from the perspective of the entire transmission system rather than focusing on an individual component. However, to obtain the temperature distribution of the gearbox, many measuring points need to be set on the parts, which weakens the convenience of the thermal network method. Even with sufficient temperature measuring points installed, it is difficult to visually present the temperature distribution of the gearbox.

The thermal equilibrium characteristics of an HST gearbox are typical of thermal multiphase flow coupling, involving multiscale complex physical phenomena such as fluid flow and conjugate heat transfer. A literature review revealed that a single thermal analysis method is insufficient for comprehensively predicting and characterizing the temperature distribution of a gearbox. In this study, a multiphysical field coupling model integrating a finite element model (FEM) and a TNM model is developed. The BoundaryToFEM unit is used to realize data exchange between the FEM and TNM, and the heat transfer and heat dissipation mechanisms of the gearbox are systematically analyzed. The purpose is to accurately predict the temperature distribution of the gearbox and provide a theoretical basis for optimizing the thermal management strategy. The reliability and accuracy of the proposed model are verified via a full-scale running-in experiment of an HST gearbox. In addition, numerical simulations were carried out to analyze the mechanism of thermal equilibrium of the gearbox from the perspective of heat generation and dissipation. The effects of the gear speed and convective HTC of the inner and outer walls of the gearbox on the thermal equilibrium characteristics are systematically studied. In the future, the influences of different environmental conditions, such as the external air flow speed and temperature, on the heat dissipation performance of the gearbox should be considered, and the thermal conductivity of the gearbox should be optimized to further reduce the thermal equilibrium temperature.

2. Methodology

2.1. MPS method and governing equations

The moving particle semi-particle (MPS) method is a CFD modeling technique in which moving particles are used instead of meshing to discretize fluid media. The rapid rotation of the gears causes the lubricant to exhibit substantial splashing, crushing, merging, and other flow behaviors. Traditional mesh-based CFD methods require specific meshing techniques to capture these small and complex oil flow behaviors. In contrast, only the fluid medium needs to be discretized in the MPS method rather than the entire fluid domain through which the fluid may flow. Therefore, the MPS is widely applied to address flow problems involving large deformations and strong nonlinearity in free liquid surfaces.

For a continuous, isothermal, and incompressible Newtonian fluid, the specific forms of the mass and momentum conservation equations in the MPS are as follows [55]:

$$\frac{\partial \rho}{\partial t} + \nabla \bullet (\rho \boldsymbol{u}) = 0 \tag{1}$$

$$\frac{Du}{Dt} = -\frac{1}{\rho}\nabla p + \nu \nabla^2 \boldsymbol{u} + \boldsymbol{g} \tag{2}$$

where ρ is the fluid density, t is time, $\boldsymbol{u}$ is the velocity vector, p is pressure, ν is the fluid viscosity coefficient, and $\boldsymbol{g}$ is the acceleration due to gravity.

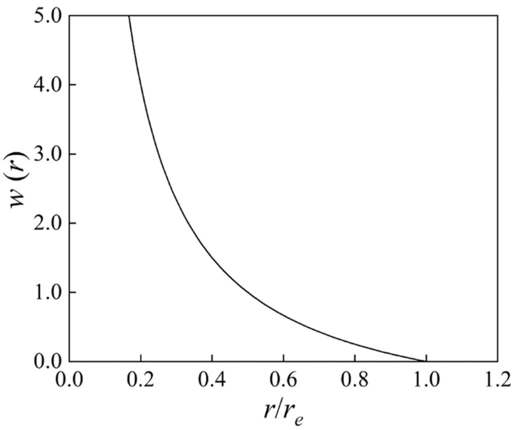

Fig. 1. Kernel function model.

The positional coordinates for fluid particles change continuously in the MPS, and the mutual effects among the particles are evaluated by a kernel function. A model of the kernel function is illustrated in Fig. 1. When $r < r_e$, an interaction force exists between two particles. When $r \geq r_e$, no interaction force occurs between two particles. An expression for the kernel function is given as follows [56]:

$$w(r) = \begin{cases} \frac{r}{r_e} - 1, (r < r_e) \\ 0, (r \geq r_e) \end{cases} \tag{3}$$

where r represents the distance between two particles and r_e denotes the particle influence radius.

The particle number density reflects a localized density characteristic of the fluid medium. The incompressibility of the fluid is maintained by ensuring that the particle number density n_i is constant. n_i is a summation of the kernel function weights in the particle action range and is expressed as follows [57]:

$$n_i = \sum_{j \neq i} w\left(\left|\vec{r}_j - \vec{r}_i\right|\right) \tag{4}$$

where ri(?)$^?$*ri* and rj(?)$^?$*rj* are the position coordinate vectors of the particles.

For the thermal characteristics analysis model of the gearbox, the MPS is used to analyze the fluid flow, and the TNM is employed to calculate the average temperature of the gearbox components when they reach thermal equilibrium. The FEM is utilized to further solve for the temperature characteristics of the gearbox. The controlling equation of the transient thermal conduction in solid components is expressed as follows [58]:

$$\rho_s C \frac{\partial T}{\partial t} = \lambda \left(\frac{\partial^2 T}{\partial x^2} + \frac{\partial^2 T}{\partial y^2} + \frac{\partial^2 T}{\partial z^2} \right) + Q \tag{5}$$

where ρ_s is the solid density, C is the specific heat capacity, λ is the thermal conductivity, t is time, T is temperature, and Q is the interior heat source, which is the source term.

2.2. Heat generation

The HST gearbox is a fixed-axis gear transmission device. The heat generated during operation primarily arises from friction power loss in different friction pairs, including gear meshing, oil churning, and bearing friction.

2.2.1. Gear meshing power loss

During engagement, a gear tooth periodically enters the gap at the root of the opposing gear tooth. This action leads to a rapid reduction in the volume between the teeth, forcing the lubricant from the gap. Fig. 2 shows a schematic illustration depicting a pair of gears at different meshing positions. S_{ij}^p denotes the squeezing side area of gear i in squeezing region j at meshing position p. The shape is determined by the involute gear profile and root profile, and the quantity depends on the engagement ratio of the mated gears.

A 3D model of the gear pair is built, and the correct meshing is detected by the center distance. A Boolean operation is used to separate the gap between the gear teeth and to quantify the area of the extrusion side. The lubricant in the extrusion region is assumed to be incompressible, and the gap between the tooth faces in the axial direction is ignored; that is, the lubricant only flows out of the side gaps. The velocity at which the lubricant is extruded is expressed as follows [59]:

$$v_{ij}^p = \frac{\Delta V}{S \Delta t} = \frac{\left(V_{ij}^p - V_{ij}^{p-1}\right)}{2 S_{ij}^p \Delta \theta} \tag{6}$$

where V_{ij}^p represents the lubricant velocity, ΔV represents the change in volume, Δt represents the change in time, and $\Delta \theta$ represents the change in angle.

After the velocity of lubricant extrusion is determined, the Bernoulli principle is used to calculate the pressure. The loss in extrusion power equals the product of the lubricant pressure and the volume change rate:

$$p_{ij}^p = p_{ij}^{p-1} + \frac{1}{2} \rho \left(\left(v_{ij}^p \right)^2 - \left(v_{ij}^{p-1} \right)^2 \right) \tag{7}$$

$$P_{ij}^p = \frac{p_{ij}^p \Delta V}{\Delta t} = \frac{p_{ij}^p \left(S_{ij}^p - S_{ij}^{p-1} \right) b \omega_i}{\Delta \theta} \tag{8}$$

where P_{ij}^p is the squeezing power loss produced by the jth squeezing side area of gear i at meshing position p and ω_i is the angular velocity of gear i. Applying the identical calculation procedure to the remaining extrusion side regions of the mated gear yields the total extrusion power loss. By dividing this value by the number of rotation positions m, the mean meshing power loss P_{m} can be calculated as follows:

$$P_{\mathrm{m}} = \frac{1}{m} \sum_{0}^{p} P_{ij}^p \tag{9}$$

Given the assumption that the entire heat produced by the meshing power loss is passed to the gears, the heat to be applied to the input gear

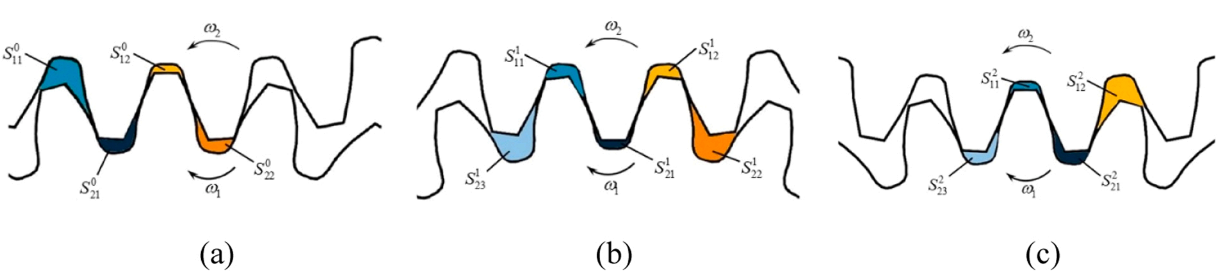

Fig. 2. Schematic diagram of the gear pairs at different meshing positions. (a) p = 0, 0°; (b) p = 1, 7.2° and (c) p = 0, 14.4°.

and the output gear are P_{mi} and P_{mo}, respectively. Heat is dissipated to the casing via the processes of thermal convection and conduction. The gear pair heat distribution coefficient β is introduced to distribute P_{m} as follows [60]:

$$\beta = \sqrt{\lambda_{\mathrm{i}}\rho_{\mathrm{i}}c_{\mathrm{i}}v_{\mathrm{i}}} \Big/ \left(\sqrt{\lambda_{\mathrm{i}}\rho_{\mathrm{i}}c_{\mathrm{i}}v_{\mathrm{i}}} + \sqrt{\lambda_{\mathrm{o}}\rho_{\mathrm{o}}c_{\mathrm{o}}v_{\mathrm{o}}}\right) \tag{10}$$

$$P_{\mathrm{mi}} = \beta P_{\mathrm{m}} \tag{11}$$

$$P_{\mathrm{mo}} = (1-\beta)P_{\mathrm{m}} \tag{12}$$

2.2.2. Gear oil churning power loss

Splash lubrication is typically implemented in HST gearboxes, and some of the gears need to be immersed in lubricant. When the gears undergo rapid rotation, the lubricant splashes onto the surfaces of the components to achieve lubrication and cooling. The gear oil churning power loss is the energy dissipated in overcoming the oil churning resistance. This power loss mainly depends on the physical characteristics of the lubricant, the volume of the lubricant and the geometric dimensions of the gear. In the MPS, the oil churning resistance is typically considered to include a vertical pressure on the gear tooth face, a lubricant viscous force and a turbulence shearing stress. The pressure gradient calculator for determining the vertical pressure on the gear tooth face is expressed as follows [61]:

$$\nabla p_i = \frac{d}{n^0}\left[\sum_{j\neq i}\frac{p_j + p_i - 2p_e}{|\vec{r}_j - \vec{r}_i|^2}(\vec{r}_j - \vec{r}_i)w(|\vec{r}_j - \vec{r}_i|) + \sum_{\substack{j'\in mirror\\ j'\in node}}\frac{p_{j'} + p_i - p_e}{|\vec{r}_{j'} - \vec{r}_i|^2}(\vec{r}_{j'} - \vec{r}_i)w(|\vec{r}_{j'} - \vec{r}_i|)\right] \tag{13}$$

where d represents the spatial dimensionality, n^0 denotes the particle number density constant, p_e represents the environmental pressure, and p_i and p_j represent the pressures of Particles i and j, respectively.

The viscous force of the lubricant may be obtained by multiplying the fluid viscosity by the Laplace velocity term, which is the second term of the momentum equation.

$$\nu\nabla^2\boldsymbol{u}_i = \nu\frac{2d}{\kappa n^0}\left[\sum_{j\neq i}(\vec{u}_j - \vec{u}_i)\omega(|\vec{r}_j - \vec{r}_i|) + \sum_{\substack{j'\in mirror\\ j'\in node}}(\vec{u}_{j'} - \vec{u}_i)\omega(|\vec{r}_{j'} - \vec{r}_i|)\right] \tag{14}$$

$$\kappa = \frac{\sum_{j\neq i}w(|\vec{r}_j - \vec{r}_i|)|\vec{r}_j - \vec{r}|^2}{\sum_{j\neq i}w(|\vec{r}_j - \vec{r}_i|)} \tag{15}$$

where κ represents the Laplace model constant, and ui(?)$^?$*ui*and uj(?)$^?$*uj*are the velocity vectors of Particles i and j, respectively.

The turbulence mixing length l is employed to calculate the turbulence shearing stress τ.

$$\tau = \rho l^2\left|\frac{\partial u}{\partial y}\right|\frac{\partial u}{\partial y} \tag{16}$$

The sum of the three values is used as the counteracting force on the gear face during churning, and the product of this force and its lever arm represents the resisting moment of the gear. The churning power loss is determined by multiplying the churning resistance moment by the rotation speed. The overall churning power loss of the gearbox can be estimated as the sum of the churning power losses from each gear. The formula is as follows:

$$P_{\mathrm{ch}} = \frac{\sum_i^n T_i \times n_i}{9550} \tag{17}$$

where T_i is the oil churning resistance moment of gear i, n_i is the rotation speed, and P_{ch} is the overall oil churning power loss.

2.2.3. Bearing friction power loss

Rapid rotations of the bearing cause friction between the bearing rollers and the cone and cup, producing heat and leading to a rapid increase in the local temperature. In this study, the bearing friction power loss is calculated by employing the international standard ISO/TR 14179. The bearing friction moment may be categorized into the following two components: the friction moment originating from the lubricant viscous effect T_{vlo} and the friction moment arising from the bearing load T_{vlp} [17,18].

$$T_{\mathrm{vlo}} = \begin{cases} 1.6\times10^{-8}f_0 d_{\mathrm{m}}^3, & (\nu_{\mathrm{oil}}n_{\mathrm{b}} < 2000) \\ 10^{-10}f_0(\nu_{\mathrm{oil}}n_{\mathrm{b}})^{2/3}d_{\mathrm{m}}^3, & (\nu_{\mathrm{oil}}n_{\mathrm{b}} \geq 2000) \end{cases} \tag{18}$$

where f_0 is the bearing lubrication coefficient, which is determined by the bearing category and lubrication type. n_{b} represents the speed of the bearing cone, which is equal to the speed of the main shaft. ν_{oil} represents the kinematic viscosity of the lubricant, and d_{m} denotes the bearing nominal diameter.

The friction moment arising from the bearing load T_{vlp} is:

$$T_{\mathrm{vlp}} = 10^{-3}f_1 P_1 d_{\mathrm{m}} \tag{19}$$

$$P_1 = f_{\mathrm{c}}(X\cdot F_r + Y\cdot F_a) \tag{20}$$

where f_1 represents the friction factor, P_1 denotes the bearing dynamic load, f_{c} represents the dynamic load coefficient, F_r denotes the bearing radial load, F_a denotes the bearing axial load, X represents the radial dynamic load factor, and Y represents the axial dynamic load factor.

The bearing friction power loss P_{b} is expressed as follows:

$$P_{\mathrm{b}} = \frac{(T_{\mathrm{vlo}} + T_{\mathrm{vlp}})n_{\mathrm{b}}}{9549} \tag{21}$$

2.3. Heat dissipation

Friction heat from the bearings and gears can be transmitted to the gear shaft and the casing through thermal conduction. Additionally, heat can also be transferred to the lubricant through convection. Precision in calculating the thermal resistance related to the thermal conduction among different components and the thermal resistance related to the thermal convection between the lubricant and components is essential for thermal equilibrium analysis of the gearbox. The thermal conduction process can be calculated and analyzed via the Fourier law. The thermal resistance of the thermal conduction is affected by the specific length of the components, the material thermoconductivity and the cross-sectional area for thermal conductivity. The thermal resistance is computed via the following equation:

$$R_{\mathrm{cond}} = \frac{\delta}{k_s A} \tag{22}$$

where R_{cond} is the thermal conduction resistance, δ is the heat transfer length in the heat transmission direction, A denotes the heat transmission area perpendicular to the heat transmission direction, and k_s denotes the material thermoconductivity.

Owing to machining limitations, a small air gap consistently exists between the two contacting surfaces. Therefore, the interfacial thermal

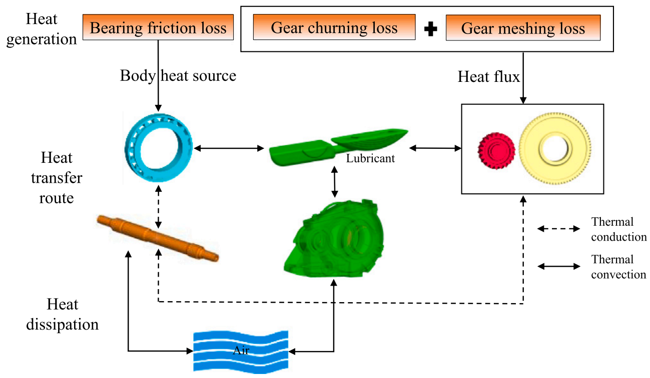

Fig. 3. Gearbox heat transfer route.

conductivity h_s must be incorporated into the thermal resistance of the two components at the contact surface. Therefore, the thermal resistance R_m between the two contact components is given by the following equation:

$$R_{\mathrm{m}} = \frac{\delta_1}{k_1 A_1} + \frac{1}{h_s A_1} + \frac{\delta_2}{k_2 A_2} \tag{23}$$

The convective heat transmission resistance R_{conv} depends on the heat exchange area A and the convective HTC h_{conv}. In addition, h_{conv} is determined by the Nusselt number Nu, the fluid thermoconductivity k_{f} and the specific length l:

$$R_{\mathrm{conv}} = \frac{1}{Ah_{\mathrm{conv}}} = \frac{1}{A}\left(\frac{l}{k_{\mathrm{f}} Nu}\right) \tag{24}$$

2.3.1. Convective HTC of the gear surfaces

Accurately calculating the convective HTCs at critical locations, such as the casing surfaces, tooth face, gear sides and bearing surfaces, is essential for thermal equilibrium analysis of the gearbox. The gear is regarded as a rotating cylinder to calculate the convective HTC on the gear surface, and the Reynolds number Re can be used to determine whether the flow condition is laminar, transitional, or turbulent. The tooth face is regarded as the circumferential surface of the cylinder, and its convective HTC is calculated according to the rotating cylinder approach [50]:

$$Nu = \begin{cases} 0.4Gr^{0.25}, & (\mathrm{Re} < 2500) \\ 0.095\left(0.5\mathrm{Re}^2 + Gr\right)^{0.35}, & (2500 \le \mathrm{Re} < 15000) \\ 0.073\mathrm{Re}^{0.7}, & (\mathrm{Re} \ge 15000) \end{cases} \tag{25}$$

$$\mathrm{Re} = \frac{\mu l}{v} \tag{26}$$

$$Gr = \frac{\rho g \Delta T l^3}{{v_{\mathrm{oil}}}^2} \tag{27}$$

where μ represents the lubricant dynamic viscosity, l denotes the specific length, Gr denotes the Grashof number and v is the flow velocity of the lubricant.

The lubricant flow on the gear ends is simplified to mimic the flow over the surface of a disk. The surface convective HTC is then calculated according to the rotating disk method [62,63]:

$$Nu = \begin{cases} 0.4\mathrm{Re}^{0.5}\mathrm{Pr}^{1/3}, & (\mathrm{Re} < 250000) \\ 0.2\mathrm{Re}^{0.5}\mathrm{Pr}^{1/3} + 0.119\mathrm{Re}^{0.8}\mathrm{Pr}^{0.6}, & (250000 \le \mathrm{Re} < 320000) \\ 0.238\mathrm{Re}^{0.8}\mathrm{Pr}^{0.6}, & (\mathrm{Re} \ge 320000) \end{cases} \tag{28}$$

$$\mathrm{Pr} = \frac{\rho c v}{\lambda} \tag{29}$$

where Pr is the Prandtl number, c denotes the lubricant specific heat capacity and λ represents the lubricant thermoconductivity.

2.3.2. Convective HTC on the surface of the casings

The convective HTCs on the internal surfaces of the casings are calculated via the following formula for forced convection heat transmission between an incompressible fluid and a flat plate [64]:

If $Re \le 1000$,

$$Nu = 0.023\mathrm{Re}^{0.8}\mathrm{Pr}^{1/3} \tag{30}$$

If $1000 < Re \le 3000$,

$$Nu = \frac{f}{8}\frac{(\mathrm{Re} - 1000)\mathrm{Pr}}{1 + 12.7\left(\frac{f}{8}\right)^{0.5}\left(\mathrm{Pr}^{2/3} - 1\right)} \tag{31}$$

$$f = 0.316\mathrm{Re}^{-0.25} \tag{32}$$

If $Re > 3000$,

$$Nu = \frac{f}{8}\frac{(\mathrm{Re} - 1000)\mathrm{Pr}}{1 + 12.7\left(\frac{f}{8}\right)^{0.5}\left(\mathrm{Pr}^{2/3} - 1\right)} \tag{33}$$

$$f = (0.79\log\mathrm{Re} - 1.64)^{-2} \tag{34}$$

The convective HTC of the external surface of the casing relies upon the airflow characteristics surrounding the gearbox. The International Standard ISO/TR 14179 provides a range of convective heat dissipation coefficients for large indoor spaces without forced cooling, ranging from 17 to 20 W/(m^2•°C). Under air-cooling conditions, the convective HTC of the external surface of the casing is a function of the fan design, cover plate design and wind speed. It is influenced primarily by the fan power and air-cooled surface area. For the numerical simulation, the convective HTC between the outer surface of the gearbox and the air was set to 18.5 W/(m^2•°C).

2.4. Heat transfer route

Fig. 3 shows the heat generation, dissipation, and transfer routes of the gearbox. The heat sources in the gearbox include bearing friction loss, gear churning loss, and meshing loss. It is generally understood that these power losses are completely converted into heat [27,65,66]. The bearing friction loss is applied to the bearing as a body heat source, whereas the gear churning loss and meshing loss are applied to the tooth surface as a surface heat source in the form of heat flux. Some of the heat generated from these sources increases the temperature of the gearbox, whereas the remainder is dissipated to the external air through convection, conduction, and radiation. Taking gear meshing loss as an example, part of the heat accumulates in the meshing area, leading to a temperature increase, while the rest is transferred to the lubricant through convection. The heat in the lubricant is transferred to the casings through convection and eventually dissipates to the external air through convection and radiation. Additionally, heat is conducted to the axles and dissipates in the same manner to the external air. The heat transfer route of other types of power loss is essentially consistent with that of gear meshing loss. Once the gearbox runs stably, heat generation and dissipation reach dynamic equilibrium, and the temperature of each component remains stable. Furthermore, owing to the small temperature differences between components in the gearbox, thermal radiation can be neglected in the simulation [53,65].

3. Model formulations

3.1. Geometric model of the gearbox

The HST gearbox investigated in this study has a maximum operating speed of 250 km/h. The HST gearbox is a single-stage parallel shaft

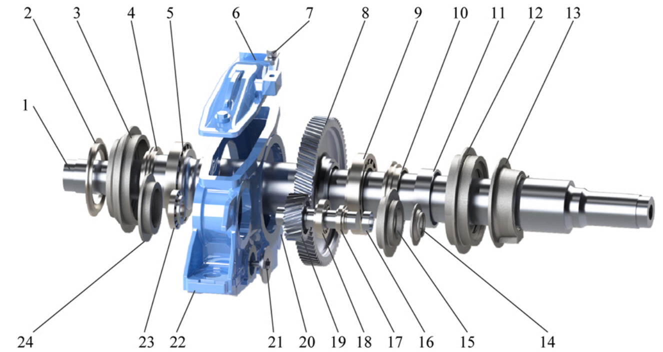

Fig. 4. Disassembled view of the HST gearbox. 1-output axle, 2-GW sealing ring A, 3-GW bushing, 4-GW sealing ring B, 5-GW bearing, 6-casing cover, 7-exhaust assembly, 8-output gear, 9-GM bearing, 10-GM sealing ring B, 11-GM sealing ring A, 12-GM bushing, 13-GM end cover, 14-PM end cover, 15-PM bushing, 16-PM sealing ring A, 17-PM sealing ring B, 18-PM bearing, 19-input gear, 20-oil level gauge, 21-magnetic bolt assembly, 22-casing body, 23-PW bearing, 24-PW end cover.

Table 1
Parameters of the transmission gear pair of the HST gearbox.

Parameter	Input gear	Output gear
Number of teeth	22	75
Modification coefficient	0.261	−0.149
Tooth width [mm]	70	
Normal module [mm]	7	
Center-to-center distance [mm]	362	
Helix angle [°]	20	
Pressure angle [°]	26	

Table 2
Parameters of the HST gearbox bearings.

Location	Model	Outer diameter [mm]	Inner diameter [mm]	Width [mm]
PM bearing	NSK-SHA/R70	150	70	38
PW bearing	NSK-SHA/R70	150	70	38
GM bearing	NSK-SHA/R205	310	205	60
GW bearing	NSK-SHA/R205	310	205	60

Table 3
Parameters of the HST gearbox bearings.

Simulation model	Velocity of the HST [km/h]	Input gear rotation speed [rpm]	Output gear rotation speed [rpm]	h_i [W/(m²•°C)]	h_o [W/(m²•°C)]
Model 01	100	−2104.07	617.19	h^*	18.5
Model 02	150	−3156.10	925.79	h^*	18.5
Model 03	200	−4208.13	1234.39	h^*	18.5
Model 04	250	−5259.83	1542.98	h^*	18.5
Model 05	200	−4208.13	1234.39	0.5 $*h^*$	18.5
Model 06	200	−4208.13	1234.39	0.75 $* h^*$	18.5
Model 07	200	−4208.13	1234.39	1.25 $* h^*$	18.5
Model 08	200	−4208.13	1234.39	1.5 $* h^*$	18.5
Model 09	200	−4208.13	1234.39	h^*	9.25
Model 10	200	−4208.13	1234.39	h^*	13.875
Model 11	200	−4208.13	1234.39	h^*	23.125
Model 12	200	−4208.13	1234.39	h^*	27.75

Note: h^* represents the convective HTC of the nonuniform distribution inside the gearbox.

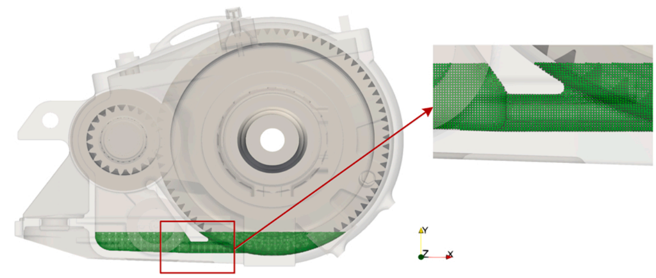

Fig. 5. Flow field model of the HST gearbox.

Table 4
The parameters of the 75W-90 lubricant [67,68].

Parameter	Value	Test method
Density at 15°C [kg•m^{-3}]	867	DIN 51757
Kinematic viscosity at 40°C [mm^2•s^{-1}]	116	ASTM D445
Kinematic viscosity at 100°C [mm^2•s^{-1}]	16.6	ASTM D445
Thermal conductivity [W/(m•°C)]	0.1253	DB61-T
Specific heat capacity [J/(kg•°C)]	1943	DSC

transmission system, and splash lubrication is implemented. The components of the gearbox include the casing, transmission gear pair, bearings, axles, and axle end accessories. Fig. 4 shows the high-fidelity 3D geometry of the gearbox. The gearbox features an integral casing consisting of a casing body and a casing cover. The output gear serves as the oil churning gear. Table 1 lists the primary characteristics of the transmission gear pair. The gearbox bearings are labeled pinion motor (PM) bearings, pinion wheel (PW) bearings, gear motor (GM) bearings, and gear wheel (GW) bearings based on their locations. The bearing models and parameters are presented in Table 2.

3.2. Simulation conditions

Twelve simulation models are developed and used to explore the thermal equilibrium characteristics of the HST gearbox, with a focus on the impact of the gear rotation speed, the convective HTC between the components and lubricant h_i, and the convective HTC between the outer surface of the gearbox and the air h_o on the gearbox thermal equilibrium. The parameters of the developed simulation models of gearbox thermal equilibrium are shown in Table 3. Models 01–04 are used to investigate the thermal equilibrium of the gearbox at different gear rotating speeds. h_i and h_o are scaled by various multiples to further analyze the heat dissipation properties of the gearbox. Models 05–08 are used to scale the nonuniform h_i of Model 03 by factors of 0.5, 0.75, 1.25 and 1.5. Models 09–12 are used to scale the h_o of Model 03 by different multiples.

3.3. Flow field model in the gearbox

The high-fidelity 3D geometry model of the gearbox is imported into shonDy 2.5.0. The lubricant is discretized with tiny particles. The established flow field model is illustrated in Fig. 5. Lubrication and cooling of the HST gearbox are accomplished using 75W-90 lubricant. Table 4 displays the physical properties of the 75W-90 lubricant.

To more accurately capture the flow field characteristics of the gearbox, the bearing motion is considered in the flow field model of the gearbox. The inner ring rotation of the bearing drives the rollers and cage to rotate. To simplify the computational model and reduce the complexity of the boundary conditions, the self-rotation of the bearing is neglected. The rolls and cage of the bearing are treated as a whole, and the calculation formula for their revolution speed is [69]:

$$n_m = \frac{1}{2}n_b\left(1 - \frac{D_b\cos\alpha}{d_m}\right) \tag{35}$$

Table 5
Particle size independence statistics.

Particle radius [mm]	Particle quantity	Output gear churning loss [W]	Error	Simulation time [h]
1.5	87,463	1390.45	6.19 %	28.86
1.25	154,245	1551.20	4.65 %	61.52
1	304,796	1451.96	2.04 %	129.38
0.75	730,053	1482.23	–	372.77

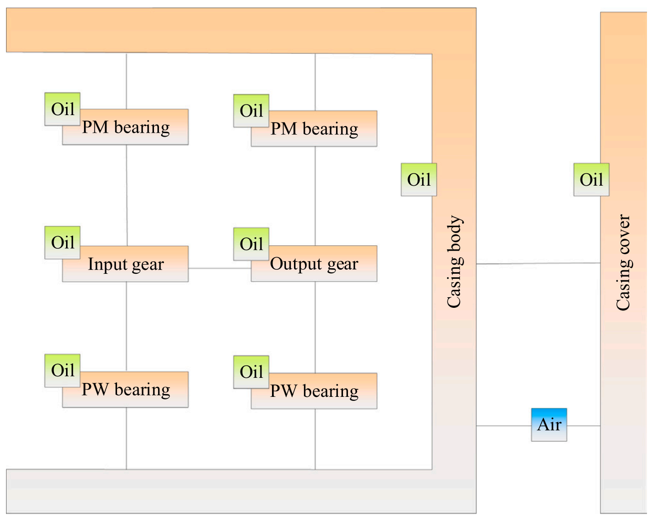

Fig. 6. Schematic diagram of the structural connection and heat transmission relationship between the gears, bearings, and casings.

where n_b is the rotational speed of the bearing cone, D_b represents the diameter of the rolling element, α is the contact angle of the bearing, and d_m denotes the pitch diameter.

The particle size is an important parameter in simulating the flow field. In theory, a smaller particle size enhances the discretization effect of the lubricant, enabling better simulation of its flow characteristics. However, excessively small particle sizes result in countless particles, demanding a very long computational time. Notably, halving the particle size requires more than 8 times the quantity of particles to fill the same amount of lubricant. A lubricant with a medium liquid level was discretized using four particles of different sizes. A numerical simulation was subsequently conducted to analyze the internal flow field. Taking the output gear churning loss as the characteristic parameter, the churning loss and the simulation time obtained for different sizes of particles are shown in Table 5. The power loss difference between particles with a 1 mm radius and those with a 0.75 mm radius is 2.04 %, but this difference is associated with a notable increase in the computation time. Hence, lubricant particles with a 1 mm radius were selected for subsequent simulations.

3.4. Thermal network model of the gearbox

According to the composition and heat transfer pathway of the gearbox, the structural connections between the gears, bearings, and casing, as well as their heat transmission relationships with the lubricant and air, are shown in Fig. 6. The heat generated by the gears and bearings is partially transferred to the casing body by thermal conduction, and the remaining portion is transferred to the lubricant through thermal convection. The flowing lubricant, which serves as a heat transfer medium, additionally transfers heat to the casing via thermal convection. Thermal conduction occurs between the casing body and the casing cover, leading to the ultimate dissipation of heat to the surrounding atmosphere through thermal convection.

The gears, bearings, casings, lubricant and air are converted into nodes, and the connection heat resistance is added between them to construct the TNM, as shown in Fig. 7. The contact surfaces between the components and the lubricant are transformed by applying BoundaryToFEM units, and constant thermal resistances are used to connect with the lubricant, as shown in Fig. 7(b).

3.5. Finite element model for thermal analysis of the gearbox

The casings are made of an aluminum alloy, the gears are composed of alloy steel, and the shaft end accessories are composed of C45 steel. The physical characteristics of the materials are detailed in Table 6. The internal surfaces of the casings, tooth ends and faces, bearing front faces, and other surfaces in contact with the lubricant should be mapped to the convective HTCs from the flow field simulation results. The convective HTCs mapped by these surfaces exhibit distributions rather than fixed values. An HTC for natural air convection is applied to the surface of the gearbox in contact with the air, aligning with the gearbox running-in experiment.

The geometric model of the gearbox is divided by a tetrahedral mesh to develop the FEM for thermal analysis. To reduce the influence of the mesh size on the simulation results, tetrahedral meshes of 9 mm, 7 mm, 5 mm, and 3 mm are used, with the corresponding numbers of elements in the FEM being approximately 2.1 million, 2.5 million, 3.4 million, and 23.7 million, respectively. The mesh independence test condition is set as follows: the HST runs at 200 km/h, the input gear speed is −4208.13 rpm, and the output gear speed is 1234.39 rpm. To maintain consistency with the heat dissipation boundary conditions of the gearbox running-in experiment, the heat dissipation coefficient of the gearbox surface is set to 18.5 $W/(m^2 \bullet {}^\circ C)$. Multiple simulations were conducted under these conditions, with the temperatures of the bearing cups and lubricant as variables. Table 7 shows the statistical data of the mesh size independence test. When the mesh size is reduced to 5 mm, the errors between the simulation and running-in experimental results remain within an acceptable range, and the deviations between the temperatures of the bearing cups and the lubricant obtained through simulation and the experimental values are less than 5 %. Accounting for both accuracy and calculation efficiency, a 5 mm mesh was finally selected to establish the FEM for thermal analysis, with a total of approximately 3.4 million elements, as shown in Fig. 8.

In this study, the governing equation for heat transfer in gearbox components is based on the heat diffusion equation:

$$\nabla \bullet (k \nabla T) + Q = 0 \tag{36}$$

where k is the thermal conductivity of the material, T is the temperature distribution, and Q represents internal heat generation. The strong form of this equation requires the solution T to have continuous second-order derivatives, which is not always feasible in numerical computation. Therefore, the equation is transformed into a weak formulation, which reduces the order of the derivatives and allows for easier numerical treatment.

The weak formulation is obtained by multiplying the governing equation by a test function ϕ, integrating over the domain Ω, and applying Green's theorem to reduce the order of differentiation:

$$\int_\Omega \phi(\nabla \bullet (k\nabla T) + Q) d\Omega = 0 \tag{37}$$

This results in the weak form:

$$\int_\Omega k \nabla \phi \bullet \nabla T d\Omega = \int_\Omega \phi Q d\Omega + \int_\Gamma \phi k \nabla T \bullet n d\Gamma \tag{38}$$

where Γ is the boundary of the domain and n is the outward unit normal on Γ. This weak formulation reduces the required smoothness of the solution, making it suitable for finite element discretization.

In the finite element method, the domain Ω is discretized into

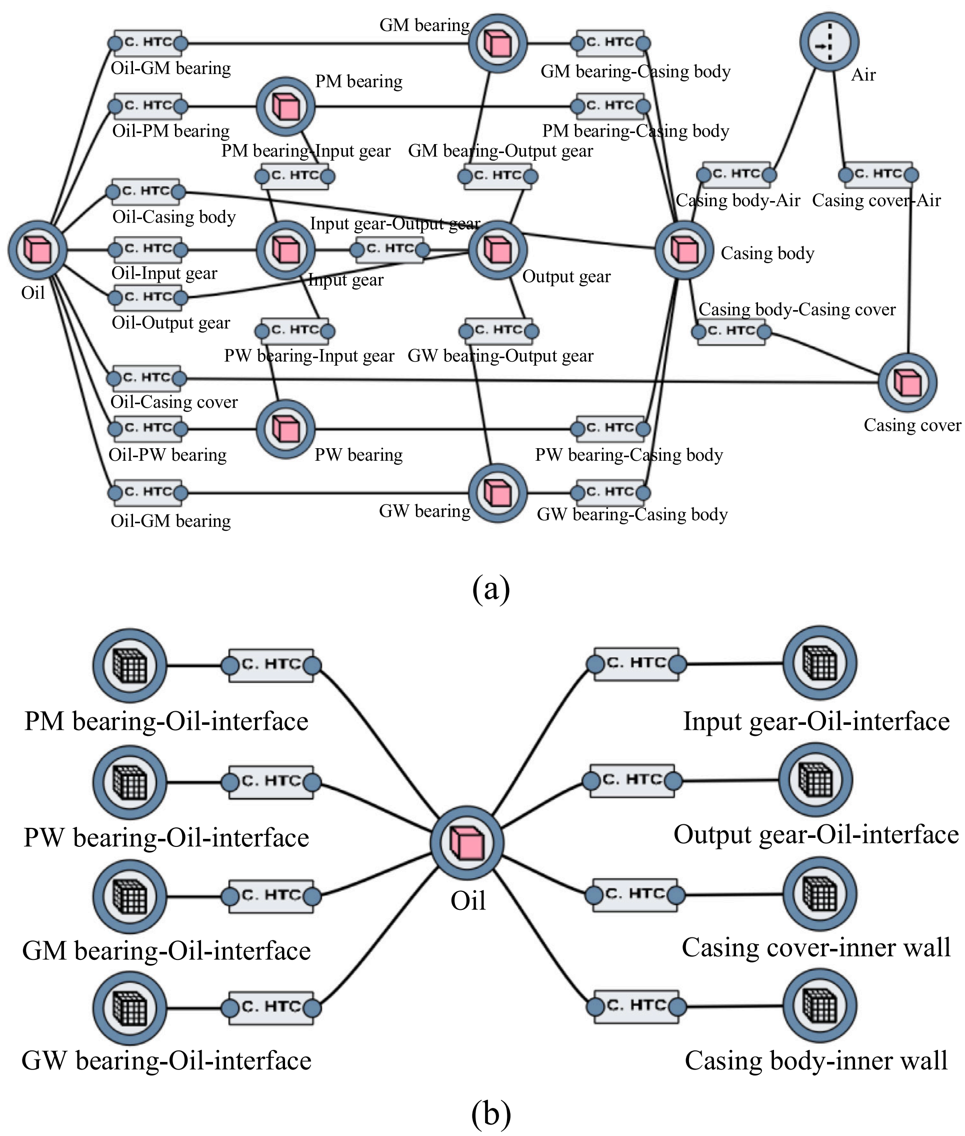

Fig. 7. Gearbox thermal network model. (a) Overall thermal network of the gearbox and (b) thermal network between the lubricant and its components.

Table 6
Physical parameters of the gearbox materials.

Name	Type	Density [kg/m^3]	Specific heat capacity [J/(kg·K)]	HTC [W/(m·K)]
Gears	18CrNiMo7–6	7850	440	52.2
Casing	AlSi7Mg0.3	2250	210	231
Shaft end accessories	C45	7850	460	42.7

tetrahedral elements, and the temperature T is approximated as a linear combination of basis functions N_i associated with the mesh nodes:

$$T(x) = \sum_i N_i(x) T_i \tag{39}$$

Substituting this approximation into the weak formulation results in a system of algebraic equations for the nodal temperatures T_i, which is solved numerically. The resulting temperature distribution across the gearbox components is then used to analyze the thermal equilibrium characteristics.

3.6. Coupling process of the finite element thermal network model

In this study, the CFD model of the flow field in the gearbox, the FEM for thermal analysis, and the TNM of the gearbox are separately established. The model coupling process is shown in Fig. 9. The MPS is used for numerical simulation of the internal flow field, obtaining the churning loss and lubricant flow state. In shonDy, the h_i is calculated based on the flow velocity of the lubricant at the surface. The power losses are calculated based on the gearbox operating conditions via evaluation methods for bearing friction and gear meshing. Typically, these power losses are assumed to be entirely converted into heat, acting as heat sources in the FEM for thermal analysis. Gear meshing and churning loss are considered together, distributed based on the β, and applied to the tooth surfaces as a surface heat flux. The Q_b calculated according to the standard ISO 14179–1 is distributed among the cone, cup, rollers and cage based on their respective volumes and is applied as a body heat source in the FEM for thermal analysis. The surface mesh from the volume mesh group of the FEM for thermal analysis is extracted and used as the 2D surface mesh in the CFD model of the gearbox flow field. Therefore, there is no tolerance between the meshes on the surface of the CFD model and the FEM. The convective HTC obtained via the CFD model can be directly mapped to the FEM for thermal analysis in the

Table 7
Mesh size independence statistics.

	Element size/mm	Element quantity	Location	PM bearing	PW bearing	GM bearing	GW bearing	Lubricant
Simulation	9	2055,827	Temperature [°C]	111.815	116.261	108.962	110.715	108.329
			Error [%]	10.38	11.13	12.53	11.86	13.97
	7	2500,114	Temperature [°C]	108.311	111.256	102.118	104.262	101.059
			Error [%]	6.92	6.34	5.46	5.34	6.32
	5	3364,407	Temperature [°C]	104.198	107.789	99.582	101.184	98.134
			Error [%]	2.78	2.94	2.76	2.18	3.14
	3	23,733,107	Temperature [°C]	103.737	107.194	98.977	100.732	97.69
			Error [%]	2.41	2.46	2.22	1.77	2.78
Experiment	–	–	Temperature [°C]	101.3	104.62	96.83	98.98	95.05

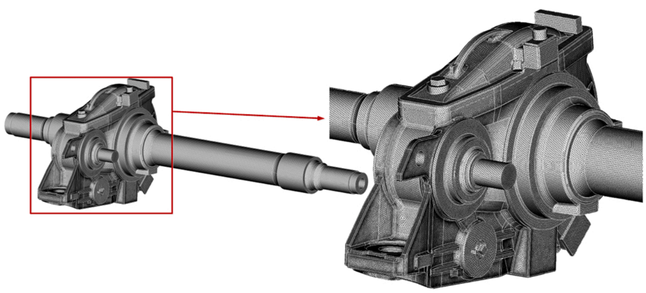

Fig. 8. FEM for the thermal analysis of a gearbox.

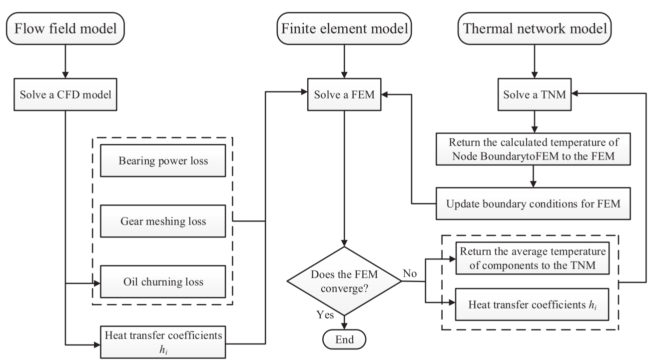

Fig. 9. Calculation flowchart of the FETNM.

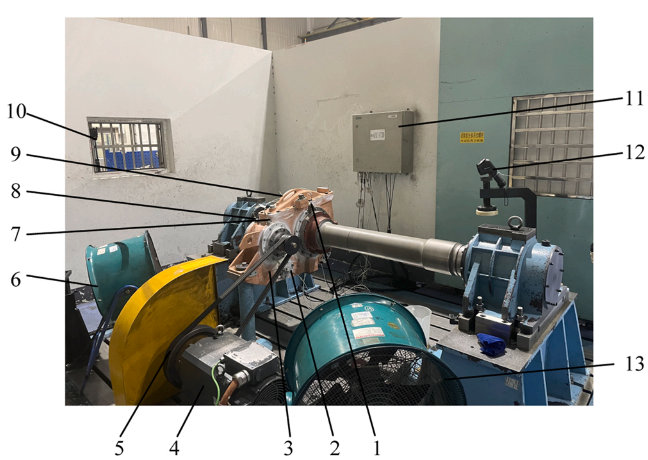

Fig. 10. Running-in test system for an HST gearbox.

form of a physical field to define the convective heat transfer boundary conditions. The nonrotating surface can directly map the quasi-steady state results of the CFD model. For the rotating surface, it is necessary to map the distribution of h_i in the initial time step and the quasi-steady

Table 8
HST gearbox running-in test system components.

No.	Description	No.	Description
1	GM-bearing temperature sensor	8	PW-bearing temperature sensor
2	Lubricant temperature sensor	9	GW-bearing temperature sensor
3	Tested gearbox	10	Infrared thermography K20
4	High-speed motor	11	Temperature acquisition system
5	Belt drive	12	Infrared thermography H13
6	Cooling fan A	13	Cooling fan B
7	PM-bearing temperature sensor		

Table 9
Technical parameters of the infrared thermography system.

Parameter	HIKMICRO H13	HIKMICRO K20
Infrared resolution [pixel]	192 * 144	256 * 192
Temperature measurement range [°C]	−20–550	−20–400
Measurement precision [°C]	±2	±2
Frame frequency [Hz]	25	25

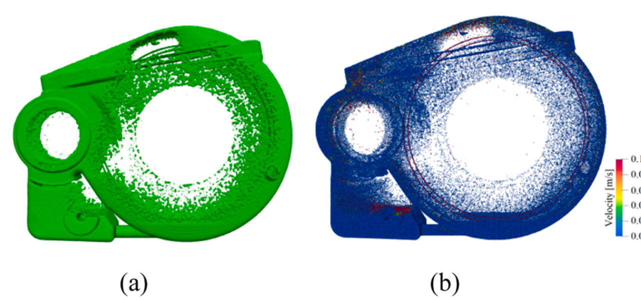

Fig. 11. Distribution and flow characteristics of the lubricant in Model 03. (a) Isosurface of the lubricant and (b) velocity of the lubricant particles.

state time step to ensure that the corresponding relationships of the nodes in the mapping process are consistent. The convective heat transfer boundary conditions between the gearbox surface and the air can be set in the FEM by defining the heat dissipation coefficients of the casing and axle surfaces.

The TNM can quickly obtain the average temperature of each component of the gearbox, whereas the FEM is used to calculate the temperature distribution. The FEM is solved, and the average temperature of each component is used as the temperature of the nodes in the TNM. The h_i is used to solve the thermal resistance between the component and the lubricant. The solution process of the TNM is equivalent to solving a set of linear equations. The whole calculation process is very efficient, and the results can be obtained quickly. The temperatures of the component nodes obtained from the TNM are mapped to the FEM through the BoundaryToFEM unit, and the FEM is solved again after updating the boundary conditions. The process is iterated multiple times until the residual of the thermal equilibrium equation is less than 10^{-6}, at which point the calculation is terminated.

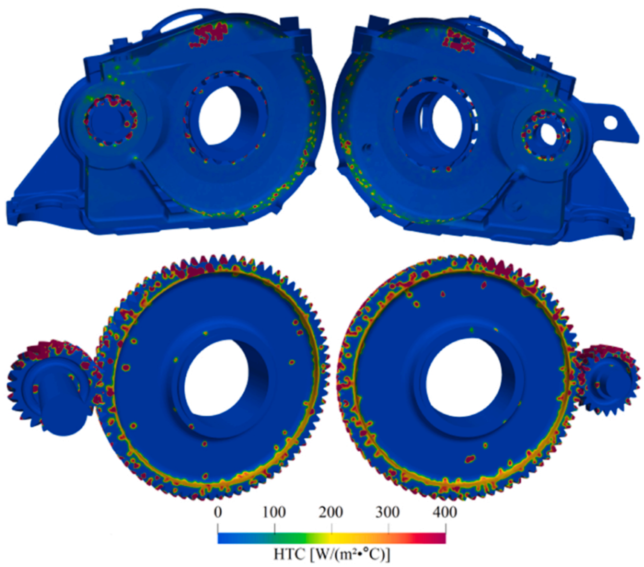

Fig. 12. Cloud map of the convective HTC inside Model 03.

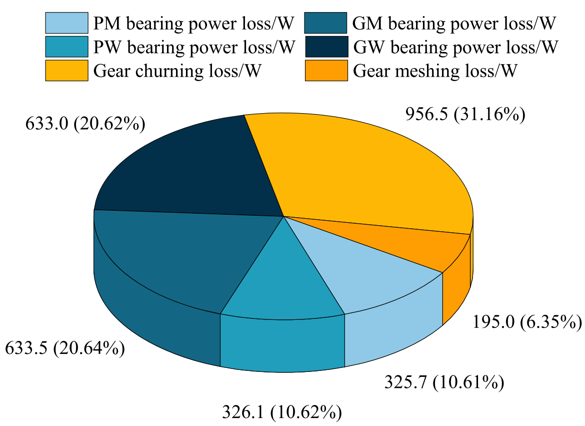

Fig. 13. Power loss and proportion of each part of Model 03.

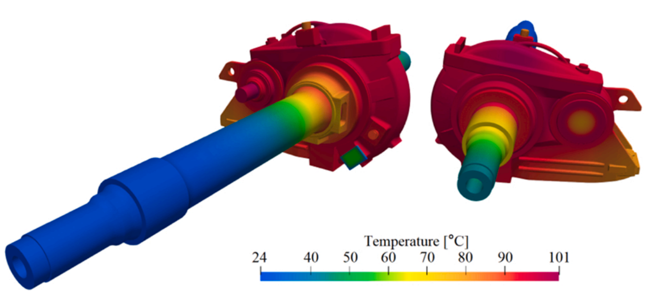

Fig. 14. Surface temperature distribution of the gearbox for Model 03: simulation results.

4. Experimental apparatus

To evaluate the performance of the FETNM, temperature rise running-in experiments were performed for an HST gearbox via a specialized test system, as depicted in Fig. 10. The running-in experimental system for the HST gearbox includes the tested gearbox, a high-speed motor, a belt drive, and a control system, which are all designed to replicate real operating conditions. The tested gearbox is supported in a 3-point manner: the two ends of the axle are fixed on the installation base through the process axle box. The lower part of the gearbox is secured by a fixed support rod. The high-speed motor transmits power through the belt drive, which drives the input gear, allowing the system to run as intended under test conditions. Table 8 provides a comprehensive component list of the gearbox running-in test system, numbered to match their corresponding elements in Fig. 10, ensuring clarity and completeness in the experimental configuration.

Temperature sensors are strategically placed to monitor the temperatures of the bearing cups and lubricant, whereas infrared thermographs are used to capture the surface temperature field. A PT100 industrial thermocouple, with a precision class of 0.15 and a measurement range of −200–200 °C, is used for accurate temperature measurement. The technical specifications of the infrared thermography equipment utilized in the system are detailed in Table 9.

To simulate natural convection and minimize the influence of external factors on the thermal dissipation characteristics of the gearbox, cooling fans are deactivated throughout the experiment. The sampling frequency of the temperature sensors is set to once per minute. According to the HST gearbox running-in experimental outline, if the temperature variation of the lubricant remains within 3 °C over a 20-min period, the gearbox is considered to have achieved thermal equilibrium, and the test is concluded [70]. Once the lubricant temperature cools to room temperature, the subsequent running-in experiment can proceed.

5. Results and discussion

5.1. Analysis of the thermal equilibrium mechanism of the gearbox

The thermal equilibrium of the gearbox is the state of dynamic balance during operation, where the heat generated from gear meshing, bearing friction, and oil churning is balanced with the heat dissipated through heat dissipation of casings, oil circulation, and other cooling mechanisms. The power losses of gears and bearings, as well as the convective HTCs on the surfaces of components, depend on the flow characteristics of the lubricant. Model 03 is chosen for the analysis of the thermal equilibrium mechanisms. The input gear speed is set to −4208.13 rpm, the output gear speed is set to 1234.39 rpm, and h_o is set to 18.5 W/(m^2•°C). Fig. 11 shows the lubricant distribution and flow characteristics of Model 03. The lubricant at the bottom of the gearbox is churned up by the output gear, covering the surfaces of the components to achieve lubrication. Owing to the throttling effect of the through-hole, most of the lubricant accumulates in the oil chamber beneath the input gear.

The convective heat transfer in the gearbox is driven mainly by the lubricant circulation flow caused by the rotation of the gear, which promotes heat exchange between the heating components and the lubricant. The high-speed rotation of the gear violently agitates the lubricant, which significantly increases the flow speed and causes it to be thrown onto the inner wall of the casing, parallel to the gear axis. After impact, the lubricant adheres to these walls and continues to flow at a high speed, resulting in significantly higher convective HTCs on these walls, as shown in Fig. 12. When the lubricant level in the gearbox reaches the midline of the oil level gauge, only a small portion of the output gear is in direct contact with the lubricant, and an oil film is formed. Owing to the rapid rotation of the gear, the convective HTC on the submerged surface is significantly improved. Because of the retraction of the middle of the casing cover, the flow of lubricant is limited, which promotes its flow to the bearing along the inner wall of the casing to achieve lubrication. On the sidewalls of the casing body, the flow of lubricant is driven mainly by gravity, resulting in low speed and convective HTC on these surfaces.

In Model 03, the power loss is contributed mainly by bearing friction, accounting for 62.49 %, followed by gear churning loss and meshing loss. Fig. 13 shows the power losses and their proportions. The bearing friction losses on the input shaft are 325.7 W and 326.1 W, respectively, whereas the bearing friction losses on the output shaft are 633.5 W and

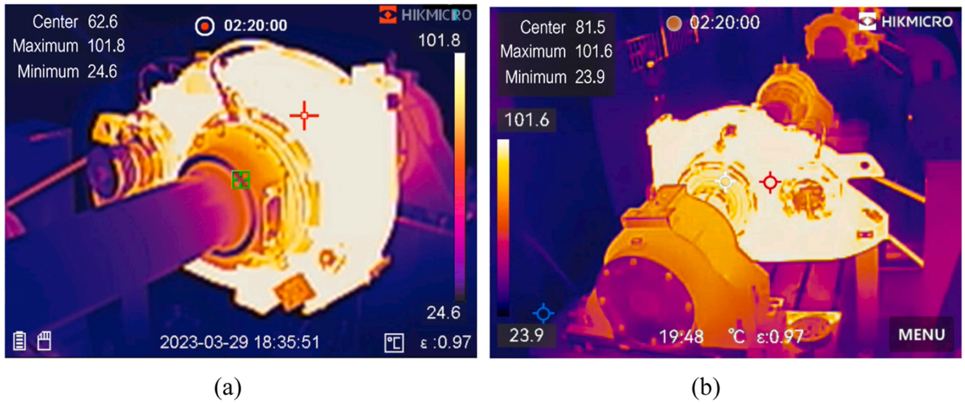

Fig. 15. Surface temperature distribution in the thermal equilibrium state for Model 03: experimental results. (a) PM and GM sides and (b) PW and GW sides.

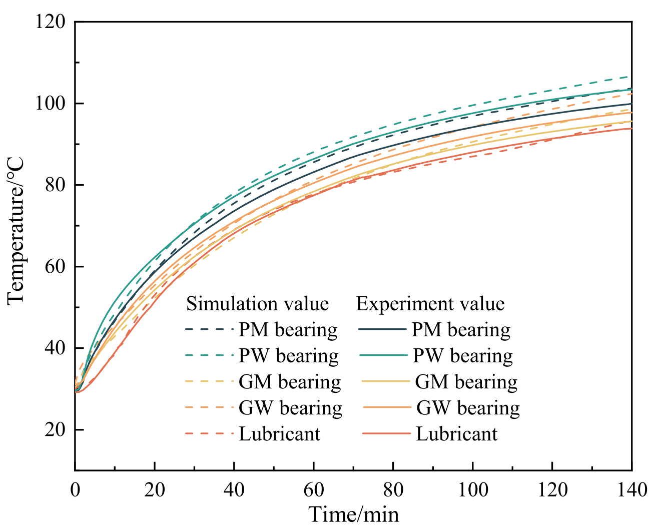

Fig. 16. Temperature rise curves of the bearings and lubricant for Model 03.

Table 10
Temperature changes in the bearings and lubricant during the final 20 min of the running test for Model 03.

Time [min]	PM bearing [°C]	PW bearing [°C]	GM bearing [°C]	GW bearing [°C]	Lubricant [°C]
120	97.43	100.91	93.07	95.23	91.35
140	99.91	103.39	95.61	97.76	93.82
Temperature difference	2.48	2.48	2.54	2.53	2.47

633.0 W. Overall, the losses of the output axis bearings are slightly greater than those of the input gear axis bearings.

Typically, gearbox power loss is assumed to be fully converted into heat. During gearbox operation, some of the heat generated by bearing friction is transmitted to the axles and the casing body through heat conduction, and the rest is transmitted to the lubricant through convection. In addition, gear churning loss and meshing loss are important heat sources. Part of the heat is transferred to the lubricant through convection, and the remaining part is transferred to the axles through heat conduction. The circulating lubricant transfers heat to the casing through convection and then dissipates it through heat exchange with the ambient air. As bearing power loss represents the largest proportion, the temperature of the bearings is notably higher than that of the other components. During the test and simulation, the gearbox is under natural cooling conditions, and the aluminum alloy casing has good thermal conductivity, resulting in a more uniform surface temperature distribution, whereas the temperature of the output axle away from the gearbox is lower. The running-in experimental results of the HST gearbox further confirmed this, showing a very uniform temperature distribution on the gearbox surface, as shown in Fig. 15. The red 'cross' indicates the highest temperature point, which continuously fluctuates near the circumferential area of the bearing.

The simulation and experimental temperatures of the bearing cups and lubricant in Model 03 are depicted in Fig. 16. Over the course of the experiment, the temperatures of the bearing cups and the lubricant steadily increased. During the period from 120 to 140 min, the lubricant temperature increases by only 2.47 °C, whereas the maximum temperature change in the bearings is 2.54 °C, as shown in Table 10. The temperature changes of the bearings and lubricant within 20 min are both less than 3 °C, indicating that the gearbox reached thermal equilibrium at the 140th minute. The simulation values exhibit a similar trend to the experimental data, with only a small difference between the simulation and experimental results at thermal equilibrium. Therefore, the FETNM for the HST gearbox established in this study is deemed

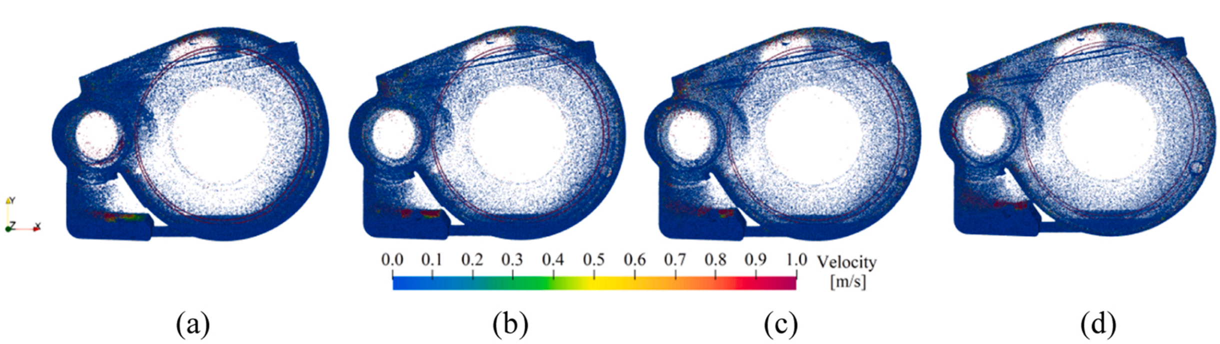

Fig. 17. Velocity contour plots of lubricant particles at different speeds. (a) Model 01, (b) Model 02, (c) Model 03 and (d) Model 04.

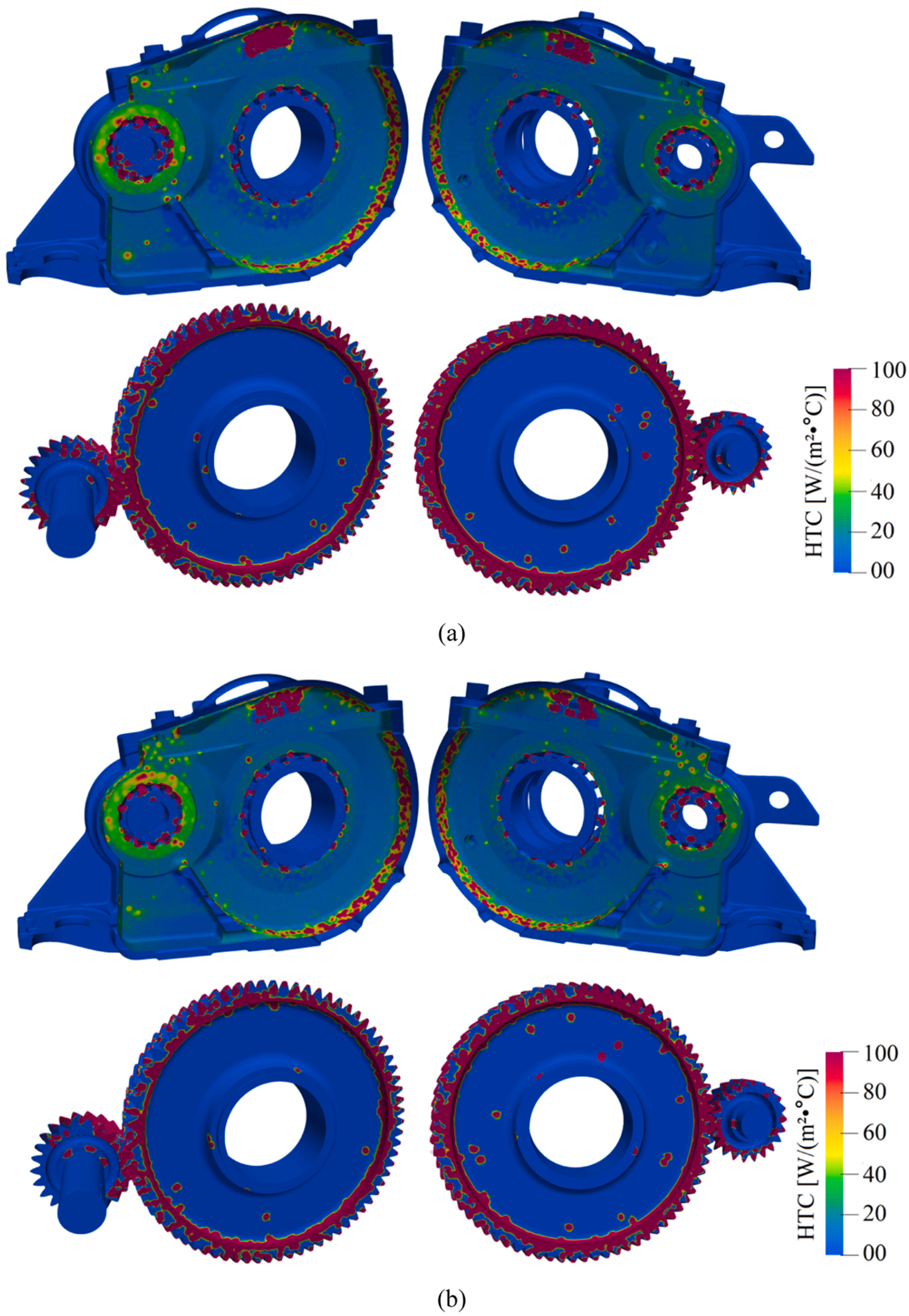

Fig. 18. Cloud map of convective heat transfer currents inside the box under different simulation speed conditions. (a) Model 01, (b) Model 02, (c) Model 03 and (d) Model 04.

accurate and dependable.

5.2. Effect of the gear rotation speed on the thermal equilibrium of a gearbox

The thermal equilibrium of the gearbox is significantly influenced by the power loss and heat dissipation boundary, both of which are governed by the flow characteristics of the lubricant. To study the impact of the gear rotation speed on the thermal equilibrium, it is assumed that h_o remains constant. This assumption is made to replicate the thermal balance state under natural convective cooling conditions. The velocity cloud images of the lubricant during gear operation at various rotating speeds are depicted in Fig. 17.

At higher rotating speeds, the increased splashing of the lubricant by the output gear results in a more uniform distribution of convective HTCs on the surfaces of the casings, as shown in Fig. 18. At higher rotating speeds, the splashing effect of the lubricant intensifies, causing more lubricant particles to be directly dispersed around the input gear, PM bearing, and PW bearing. This phenomenon increases the volume of lubricant in the chamber beneath the input gear while also enhancing the convective HTC around the PM and PW bearing areas. The high-speed rotation of the gear increases the centrifugal force acting on the

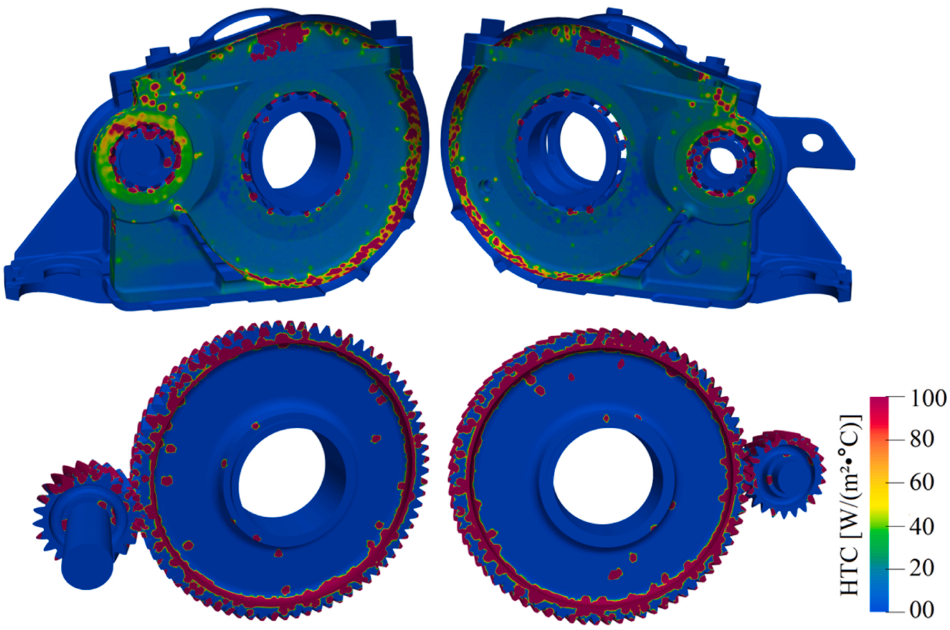

(c)

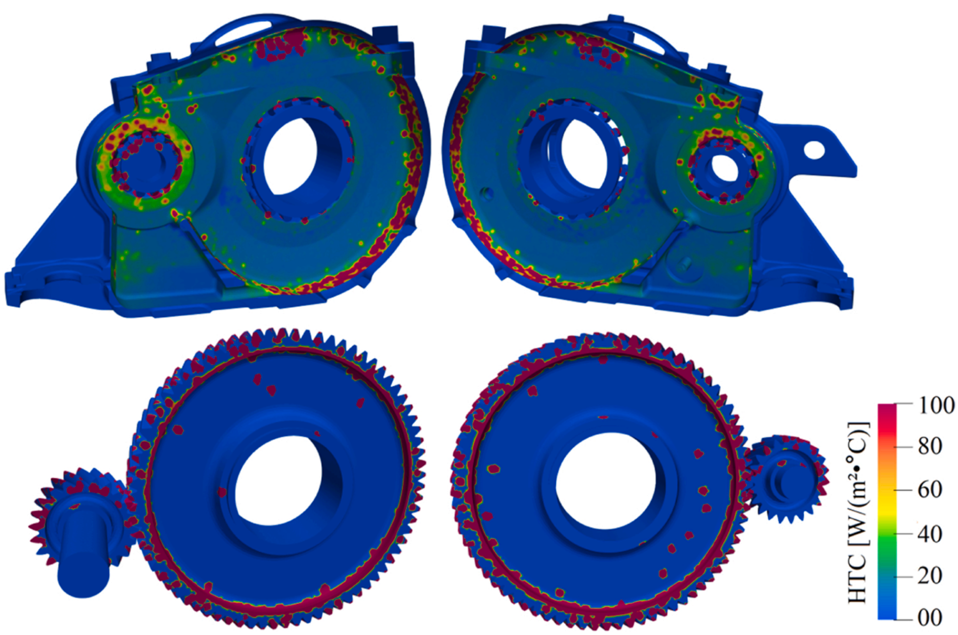

(d)

Fig. 18. (*continued*).

Table 11
Power loss of the models with different gear rotating speeds.

Model	PM bearing [W]	PW bearing [W]	GM bearing [W]	GW bearing [W]	Gear meshing [W]	Gear churning [W]	Total power loss [W]
Model 01	219.6	219.8	427.7	426.4	97.5	178.4	1569.4
Model 02	251.2	251.5	585.5	585.0	146.3	442.1	2261.6
Model 03	325.7	326.1	633.5	633.0	195.0	846.5	2959.8
Model 04	351.5	352.0	664.8	664.1	243.8	1452.0	3728.2

surface lubricant, causing the lubricant to gradually be displaced from the gear teeth, thereby reducing the lubricant coverage in these surfaces and the convective HTC.

As the gear speed increases, the power loss in various components increases, and at higher speeds, gear churning loss becomes the predominant factor. Table 11 displays the power loss of Models 01–04. When the input gear speed increased from 2104 rpm to 5259 rpm, the total power loss in the gearbox rose by 2159 W. During this process, the

Table 12
Bearing and lubricant temperatures of the models with different gear rotating speeds.

Model	Method	PM bearing [°C]	PW bearing [°C]	GM bearing [°C]	GW bearing [°C]	Lubricant [°C]
Model 01	Simulation	64.85	66.28	62.52	63.71	61.84
	Experiment	62.22	63.66	59.94	61.16	58.65
	Error	4.23 %	4.12 %	4.30 %	4.17 %	5.44 %
Model 02	Simulation	82.99	85.65	79.44	81.66	79.50
	Experiment	80.50	83.02	77.44	79.48	76.32
	Error	3.09 %	3.17 %	2.58 %	2.74 %	4.17 %
Model 03	Simulation	102.69	106.67	98.58	101.35	95.83
	Experiment	99.91	103.39	95.61	97.76	93.82
	Error	2.78 %	3.17 %	3.11 %	3.67 %	2.14 %
Model 04	Simulation	119.32	124.09	112.53	115.31	112.07
	Experiment	116.86	121.70	109.84	112.61	109.87
	Error	2.11 %	1.96 %	2.45 %	2.40 %	2.00 %

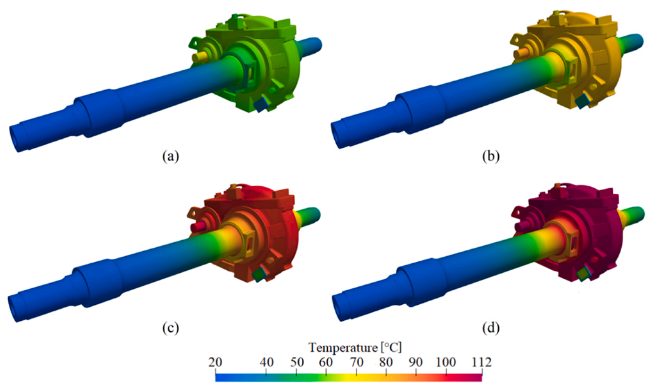

Fig. 19. Surface temperature cloud map of the gearbox under different speed simulation conditions. (a) Model 01, (b) Model 02, (c) Model 03 and (d) Model 04.

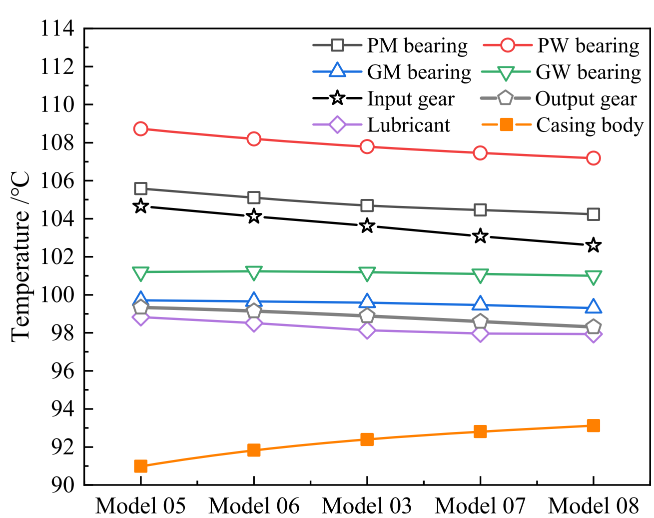

Fig. 20. Temperatures of the bearings and lubricant under different h_i.

gear churning loss increased by 1273.6 W, accounting for approximately 59 % of the total increase in power loss. Moreover, when the input gear speed exceeds 4208 rpm, churning loss surpasses the power loss generated by any single bearing, becoming a major source of power loss. Based on the findings from Otto [71], churning power loss exhibits an almost exponential relationship with speed. Therefore, at high rotation speeds, careful consideration must be given to mitigating churning loss.

The thermal equilibrium temperature of the gearbox increases with increasing gear rotation speed, mainly because of the increase in power loss. Table 12 presents the temperatures of the bearing cups and the lubricant at various rotating speeds. When the input gear speed increased from 2104 rpm to 5259 rpm, the temperature of the bearing cups rose by an average of 53.5 °C, with a more pronounced temperature rise on the input gear axle bearings than on the output axle bearings. During this process, the average temperature of the lubricant increased from 61.84 °C to 109.87 °C. Fig. 19 shows the temperature fields at thermal equilibrium for the gearbox. To facilitate comparison, the temperature fields are displayed within the range of 20–112 °C. The surface temperature of the gearbox increased from approximately 50 °C to over 110 °C, with the average temperature rising by more than 50 °C.

Table 12 further provides a comparison between the predicted and experimental temperatures for the bearings and lubricant. In Model 01, the discrepancy between the simulation and experimental results ranged from 4.12 % to 5.44 %, with the largest deviation observed in the lubricant temperature. For Models 02 and 03, the error decreased to a range of 2.14–4.17 %, and for Model 04, the error was further reduced, ranging from 1.96 % to 2.45 %. Overall, the errors presented in Table 12 remain within a narrow range, reflecting a consistent agreement between the predicted and experimental data of the established model. Although h_i increases with increasing gear rotation speed, the magnitude of this change is relatively small. h_i primarily reflects the heat exchange capability between the lubricant and components, and an increase in h_i merely strengthens the transfer of frictional heat to the lubricant. In addition, Models 01–04 simulate the thermal equilibrium characteristics of the gearbox under natural convection. h_o is a constant, and the heat dissipating ability of the gearbox remains unchanged. Therefore, the thermal equilibrium temperature of the gearbox gradually increases with increasing gear rotation speed.

5.3. *Effect of the convective heat transfer boundary on the thermal equilibrium characteristics of the gearbox*

Thermal convection in a gearbox is an essential mechanism for dissipating heat. This process involves heat exchange among the components and lubricant, as well as heat exchange between the gearbox and air. To analyze the role of these thermal convection boundaries in thermal equilibrium accurately, h_i and h_o are proportionally adjusted. h_i is provided as a distribution field, and h_o is kept constant to simulate the thermal equilibrium characteristics of the gearbox under natural convection.

Based on Model 03, h_i is scaled by factors of 0.5, 0.75, 1.25, and 1.5, corresponding to a reduction of 50 %, a reduction of 25 %, an increase of 25 %, and an increase of 50 %, respectively, resulting in Models 05–08. Fig. 20 presents the steady-state temperatures of the bearings, gears, casing body, and lubricant for the different models at thermal equilibrium. As the convective HTC between the lubricant and the components increases, the temperature of the gears, bearings and lubricants decreases, whereas the temperature of the casing body increases. Specifically, when the scale factor of h_i increases from 0.5 to 1.5, the temperature of the PM bearing decreases from 105.6 °C to 104.2 °C, the temperature of the PW bearing decreases from 108.7 °C to 107.2 °C, and

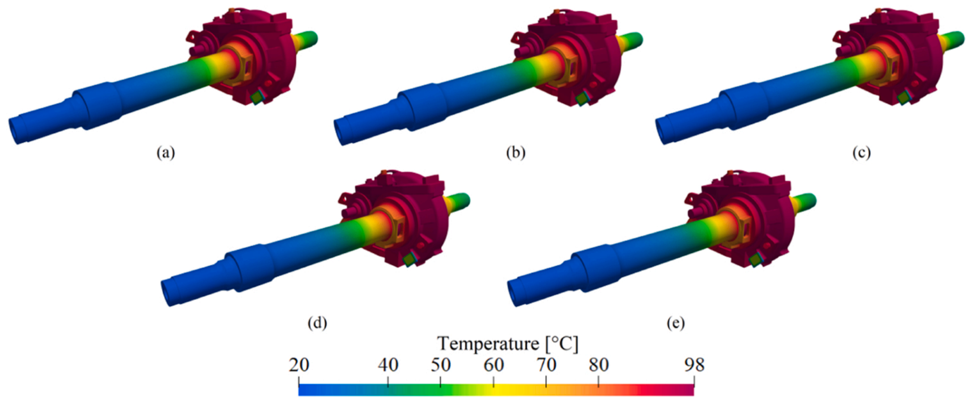

Fig. 21. Surface temperature cloud map of the gearbox under different h_i. (a) Model 05, (b) Model 06, (c) Model 03, (d) Model 07 and (d) Model 08.

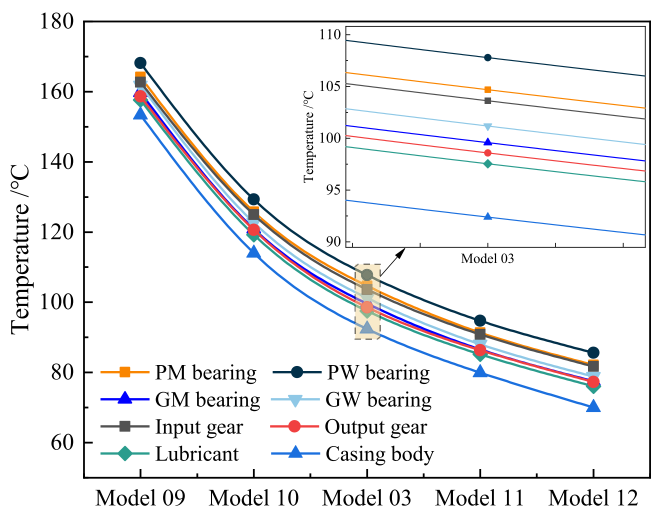

Fig. 22. Temperatures of the bearings and lubricant for different h_o.

the temperature of the input gear decreases from 104.65 °C to 102.6 °C. The temperatures of the output gear, GM bearing, and GW bearing decrease only slightly, and the decrease is smaller than that of the input gear and its adjacent bearings. This is because the high-speed rotating output gear splashes the lubricant to the area near the input gear, which accelerates the flow speed of the lubricant near the PM and PW bearings, thereby increasing the convective HTC of the surface. In contrast, the lubricant near the GM and GW bearings is affected mainly by gravity and flows slowly along the wall, resulting in a lower convective HTC. When the convective HTC is adjusted proportionally, the variation in the surface HTC near the GM and GW bearings is minimal, resulting in a temperature decrease of only approximately 0.3 °C for these bearings.

When h_i increased from a 50 % reduction to a 50 % magnification, the heat exchange capacity between the lubricant and the components gradually improved. Therefore, more heat is transferred from the gear and bearing to the lubricant, resulting in a decrease in the temperature of the gear and bearing. Moreover, the increase in h_i also enhances the heat exchange between the lubricant and the casing so that more heat is transferred from the lubricant to the casing, and the lubricant temperature is reduced from 98.83 °C to 97.93 °C. However, in Models 05–08, h_o remains unchanged; that is, the heat exchange capacity between the gearbox and the environment remains unchanged, so the average temperature of the casing body increases from 90.98 °C to 93.12 °C. Since the casings are made of aluminum alloy with excellent thermal conductivity, heat can be quickly conducted, resulting in a relatively uniform temperature distribution, as shown in Fig. 21. In addition, the continuous circulation of lubricant and heat transfer effectively reduce the temperature gradient within the gearbox, prevent local overheating, and promote a more uniform temperature distribution.

External airflow is the primary mode of heat dissipation for HST gearboxes. When analyzing the impact of h_o on the thermal equilibrium characteristics while maintaining constant power loss and h_i, a comparative analysis is performed for Models 09–12 and 03. The temperature field of the gearbox and the temperature values of the bearing cups and lubricant when the gearbox reaches thermal equilibrium are shown in Figs. 22 and 23. Increasing h_o from 9.25 W/(m^2•°C) to 27.75 W/(m^2•°C) results in a decrease in the average temperature of the gearbox from approximately 153 °C to 70 °C. The temperatures of the gears, bearings, and lubricant also decrease with increasing h_o.

When h_o increases from 50 % reduction to 50 % magnification, the

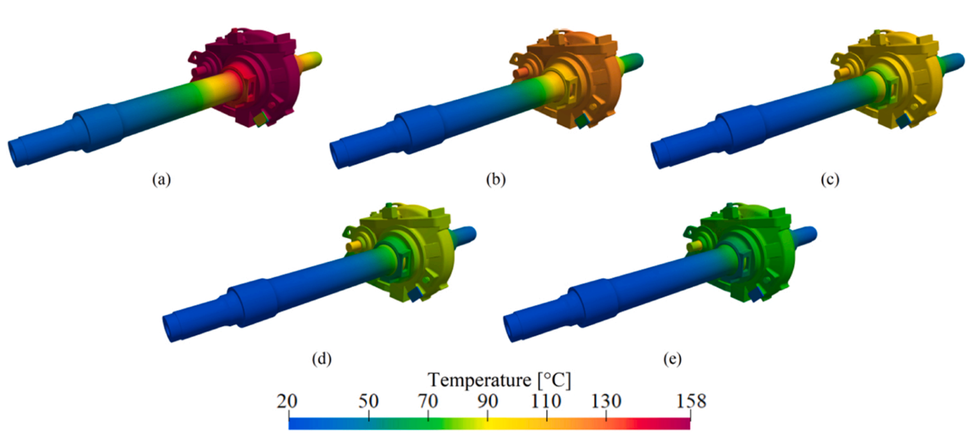

Fig. 23. Surface temperature cloud map of the gearbox under different h_o. (a) Model 09, (b) Model 10, (c) Model 03, (d) Model 11 and (d) Model 12.

heat exchange between the gearbox and the external environment is significantly enhanced so that the heat is more effectively transferred to the surrounding atmosphere, and the temperature of the casing body is reduced from approximately 153.4 °C to 70 °C. As the temperature of the casing decreases, the temperature difference between the lubricant and the casing increases. Although h_i remained unchanged, the increased temperature difference caused more heat to be transferred from the lubricant to the casings, reducing the lubricant temperature from approximately 157.7 °C to 76 °C. Additionally, the variation in the temperature difference facilitates heat exchange between the lubricant and the gears and bearings, effectively removing heat from these components and reducing their temperatures. In addition, the decrease in the casing temperature further increases the temperature difference between the bearing and the casing, improves heat conduction, and accelerates the reduction in the bearing temperature.

A comparison of the effects of h_i and h_o on the thermal equilibrium characteristics reveals that an increase in h_o can significantly reduce the thermal equilibrium temperature of a gearbox with the same scale factor. The primary function of the lubricant inside the gearbox is to transfer heat through convection rather than directly cooling the components. The flow of the lubricant helps to distribute heat evenly and prevent local overheating, but its cooling effect is limited. To reduce the overall thermal equilibrium temperature of the gearbox, h_o should be preferentially increased. Improving the design of the casing surface, such as adding fins or rib structures, can enhance air convection and further increase the heat dissipation capability of the gearbox. Additionally, optimizing the arrangement of components beneath the train to make full use of the airflow during train movement can enhance the heat transfer efficiency of the gearbox. Similarly, Yazdani et al. [72] indicated that because of the absence of active circulation, the lubricant serves for convective heat transfer rather than for cooling. The temperature distribution of the gearbox also indicates that the heat is transferred primarily to the external air through the solid components rather than being exchanged with the internal environment.

6. Conclusions and future work

Accurately assessing the thermal equilibrium of HST gearboxes is crucial for improving transmission efficiency and ensuring train safety. By combining the FEM with the TNM through the BoundaryToFEM unit, an FETNM that can be used to study the thermal equilibrium of HST gearboxes was proposed. The model provides an innovative approach for solving the fluid—solid conjugate heat transfer problem. Research has investigated the impact of the gear rotation speed and convective heat transfer boundaries on the thermal equilibrium characteristics of a gearbox. The main findings are summarized as follows:

(1) A full-scale running-in experiment of the HST gearbox was carried out at various speed levels. The error between the bearing cup temperature predicted by the FETNM and the running-in experimental results was within 2–5 %, and the maximum error between the predicted value of the lubricant temperature and the experimental results was 3.18 °C. Furthermore, the temperature distribution predicted by the FETNM was highly consistent with the infrared camera measurements. These results demonstrate that the proposed FETNM is capable of accurately predicting the thermal equilibrium characteristics of the gearbox.

(2) With increasing rotation speed, the bearing friction, gear meshing and churning power losses in the gearbox all tend to increase. When the input gear speed increased from 2104 rpm to 5259 rpm, the total power loss increased by 2159 W, and the temperature of the bearing and lubricant increased by approximately 53 °C. When the input gear speed exceeds 4208 rpm, the churning loss surpasses the power loss of any single bearing, which becomes one of the major sources of power loss in the gearbox.

(3) The influences of h_i and h_o on the thermal equilibrium characteristics of the gearbox were analyzed. With the power loss in the gearbox kept constant, when the h_i increases from a 50 % reduction to a 50 % magnification, the temperature of the components and lubricant changed by only approximately 1–2 °C. In contrast, when the same modification is applied to h_o, the thermal equilibrium temperature of the gearbox decreases by approximately 82 °C. The main function of the lubricant is to remove the heat generated by the components in time rather than to cool directly. The main heat dissipation mechanism of the gearbox is through heat exchange with the surrounding air.

The gearbox running-in experiments in this research were carried out under laboratory conditions, which are different from the actual operating conditions. In future work, the influence of external airflow outside the gearbox on the thermal equilibrium under actual HST operating conditions can be studied, with an in-depth exploration of its impact on the heat dissipation mechanism. This will provide systematic theoretical guidance and methods for optimizing the layout of components beneath the train and the design of the gearbox surface.

CRediT authorship contribution statement

Jin Siqin: Visualization, Data curation. **Liu Yi:** Visualization, Software, Data curation. **Wang Zhengyang:** Visualization, Software. **Zhang Kailin:** Validation, Supervision, Project administration, Methodology, Funding acquisition. **Shao Shuai:** Writing – review & editing, Writing – original draft, Visualization, Validation, Software, Methodology, Investigation, Formal analysis, Data curation, Conceptualization. **Yao Yuan:** Supervision, Project administration, Funding acquisition.

Declaration of Competing Interest

The authors declare that they have no known competing financial interests or personal relationships that could have appeared to influence the work reported in this paper.

Acknowledgments

This research is funded by the National Natural Science Foundation of China [grant number 52372403 and U2268211]; the Natural Science Foundation of Sichuan Province [Grant Numbers 2022NSFSC0034 and 2022NSFSC1901]; and the Independent Research and Development Project from the State Key Laboratory of Rail Transit Vehicle System [Grant Number 2022TPL_T02].

Data Availability

No data was used for the research described in the article.

References

[1] H. Chen, B. Jin, W. Chen, H. Yi, Data-driven detection and diagnosis of incipient faults in electrical drives of high-speed trains, IEEE Trans. Ind. Electron 66 (6) (2018) 4716–4725, https://doi.org/10.1109/TIE.2018.2863191.

[2] H. Dong, B. Ning, B. Cai, Z. Hou, Automatic train control system development and simulation for high-speed railways, Ieee Circuits Syst. Mag. 10 (2) (2010) 6–18, https://doi.org/10.1109/MCAS.2010.936782.

[3] Z. Wang, Z. Yin, R. Wang, Y. Cheng, P. Allen, W. Zhang, Coupled dynamic behaviour of a transmission system with gear eccentricities for a high-speed train, Veh. Syst. Dyn. 59 (4) (2021) 613–634, https://doi.org/10.1080/00423114.2019.1708008.

[4] L. Hildebrand, S. Genuin, T. Lohner, K. Stahl, Numerical analysis of the heat transfer of gears under oil dip lubrication, Tribol. Int. 195 (2024) 109652, https://doi.org/10.1016/j.triboint.2024.109652.

[5] Q. Li, P. Xu, L. Li, W. Xu, D. Tan, Investigation on the lubrication heat transfer mechanism of the multilevel gearbox by the lattice boltzmann method, Processes 12 (2) (2024) 381, https://doi.org/10.3390/pr12020381.

[6] H. Liu, T. Jurkschat, T. Lohner, K. Stahl, Determination of oil distribution and churning power loss of gearboxes by finite volume CFD method, Tribol. Int. 109 (2017) 346–354, https://doi.org/10.1016/j.triboint.2016.12.042.
[7] K. Yue, Z. Kang, M. Zhang, L. Wang, Y. Shao, Z. Chen, Study on gear meshing power loss calculation considering the coupling effect of friction and dynamic characteristics, Tribol. Int. 183 (2023) 108378, https://doi.org/10.1016/j.triboint.2023.108378.
[8] A. Kahraman, D.R. Hilty, A. Singh, An experimental investigation of spin power losses of a planetary gear set, Mech. Mach. Theory 86 (2015) 48–61, https://doi.org/10.1016/j.mechmachtheory.2014.12.003.
[9] Y. Zhao, Y. Zi, Z. Chen, M. Zhang, Y. Zhu, J. Yin, Power loss investigation of ball bearings considering rolling-sliding contacts, Int. J. Mech. Sci. 250 (2023) 108318, https://doi.org/10.1016/j.ijmecsci.2023.108318.
[10] R. Kerrouche, A. Dadouche, M. Mamou, S. Boukraa, Power loss estimation and thermal analysis of an aero-engine cylindrical roller bearing, Tribol. Trans. 64 (6) (2021) 1079–1094, https://doi.org/10.1080/10402004.2021.1958966.
[11] X. Zhu, Y. Dai, Development of an analytical model to predict the churning power losses of an orthogonal face gear, Eng. Sci. Technol. 41 (2023) 101383, https://doi.org/10.1016/j.jestch.2023.101383.
[12] F. Concli, C. Gorla, A CFD analysis of the oil squeezing power losses of a gear pair (A), Int. J. Comput. Methods Exp. Meas. 2 (2) (2014) 157–167, https://doi.org/10.2495/CMEM-V2-N2-157-167.
[13] N.E. Anderson, S.H. Loewenthal, Design of spur gears for improved efficiency, t, J. Mech. Des. 104 (4) (1982) 767–774, https://doi.org/10.1115/1.3256434.
[14] J. Yang, T. Lin, Calculation method and parameter optimization for friction power loss of the modified double-helical gear transmission, Meccanica 58 (2023) 1–23, https://doi.org/10.1007/s11012-022-01625-2.
[15] J.J. Coy, D.P. Townsend, E.V. Zaretsky, Gearing, NASA Ref. Publ. 1152 (1985).
[16] S. Li, A. Kahraman, Prediction of spur gear mechanical power losses using a transient elastohydrodynamic lubrication model, Tribol. Trans. 53 (4) (2010) 554–563, https://doi.org/10.1080/10402000903502279.
[17] ISO 14179–1, Gears – thermal capacity – part 1: Rating gear drives with thermal equilibrium at 95 °C sump temperature, (2001) 14179–1.
[18] ISO 14179–2, Gears – thermal capacity – part 2: Thermal load-carrying capacity, (2001) 14179–2.
[19] M. Yoshizaki, C. Naruse, R. Nemoto, S. Haizuka, Study on frictional loss of spur gears (concerning the influence of tooth form, load, tooth surface roughness, and lubricating oil), Tribol. Trans. 34 (1) (1991) 138–146, https://doi.org/10.1080/10402009108982021.
[20] S. Seetharaman, A. Kahraman, Load-independent spin power losses of a spur gear pair: model formulation, J. Tribol. 131 (2) (2009) 22201, https://doi.org/10.1115/1.3085943.
[21] B. SKF, The SKF model for calculating the frictional moment, SKF, 2018. ⟨https://www.skf.com/binaries/pub12/Images/0901d1968065e9e7-The-SKF-model-for-calculating-the-frictional-movement_tcm_12-299767.pdf⟩.
[22] ISO 15312, Rolling bearings – thermal speed rating – calculation, (2018) 15312.
[23] A. Palmgren, Ball and Roller Bearing Engineering, SKF industries Inc, Philadephia, 1959.
[24] D. Astridge, C. Smith, Heat generation in high-speed cylindrical roller bearings, Proc. Inst. Mech. Eng. Elasto-hydrodyn. Lubri., (1972 UK) 83-94, Leeds, UK.
[25] Timken. Timken Engineering Manual, Timken, 2016
[26] A. Popescu, L. Houpert, D.N. Olaru, Four approaches for calculating power losses in an angular contact ball bearing, Mech. Mach. Theory 144 (2020) 103669, https://doi.org/10.1016/j.mechmachtheory.2019.103669.
[27] C.M.C.G. Fernandes, P.M.T. Marques, R.C. Martins, J.H.O. Seabra, Gearbox power loss. part I: losses in rolling bearings, Tribol. Int. 88 (2015) 298–308, https://doi.org/10.1016/j.triboint.2014.11.017.
[28] A.S. Terekhov, Hydraulic losses in gearboxes with oil immersion, Russ. Eng. J. 55 (5) (1975) 7–11.
[29] R.J. Boness, Churning losses of discs and gears running partially submerged in oil, Chicago, Illinois,1989.
[30] P. Luke, A.V. Olver, A study of churning losses in dip-lubricated spur gears, Proc. Inst. Mech. Eng. Part G: J. Aerosp. Eng. 213 (5) (1999) 337–346, https://doi.org/10.1243/0954410991533061.
[31] C. Changenet, G. Leprince, F. Ville, P. Velex, A note on flow regimes and churning loss modeling, J. Mech. Des. 133 (12) (2011) 121009, https://doi.org/10.1115/1.4005330.
[33] C. Changenet, P. Velex, Housing influence on churning losses in geared transmissions, J. Mech. Des. 130 (6) (2008) 062603, https://doi.org/10.1115/1.2900714.
[32] C. Changenet, P. Velex, A model for the prediction of churning losses in geared transmissions-preliminary results, J. Mech. Des. 129 (1) (2007) 128, https://doi.org/10.1115/1.2403727.
[34] H. Liu, G. Arfaoui, M. Stanic, L. Montigny, T. Jurkschat, T. Lohner, K. Stahl, Numerical modelling of oil distribution and churning gear power losses of gearboxes by smoothed particle hydrodynamics, Proc. Inst. Mech. Eng. Part J: J. Eng. Tribol. 233 (1) (2019) 74–86, https://doi.org/10.1177/1350650118760626.
[35] D. Guo, F. Chen, J. Liu, Y. Wang, X. Wang, Numerical modeling of churning power loss of gear system based on moving particle method, Tribol. Trans. 63 (1) (2020) 182–193, https://doi.org/10.1080/10402004.2019.1682212.
[36] S. Hu, W. Gong, P. Gui, Numerical study on the churning power loss of spiral bevel gears at splash lubrication system, Lubr. Sci. 36 (4) (2024) 259–276, https://doi.org/10.1002/ls.1688.
[37] C. Bouchoule, M. Fillon, D. Nicolas, F. Baressi, Thermal effects in hydrodynamic journal bearings of speed increasing and reduction gearboxes, Proc. 24th Turbomach. Symp., (USA. 1995) Texas, USA.
[38] E. Letzelter, M. Guingand, J.P. de Vaujany, P. Schlosser, A new experimental approach for measuring thermal behaviour in the case of nylon 6/6 cylindrical gears, Polym. Test. 29 (2010) 1041–1051, https://doi.org/10.1016/j.polymertesting.2010.09.002.
[39] J. Chang, S. Liu, X. Hu, A temperature measurement method for testing lubrication system or revealing scuffing failure mechanism of spur gear, Proc. Inst. Mech. Eng. Part J: J. Eng. Tribol. 233 (6) (2019) 831–840, https://doi.org/10.1177/1350650118799927.
[40] A. Chougale, J. Bhat, M. Desai, U. Bhapkar, Effect of operating parameters of worm gearbox on lubricant oil temperature, Mater. Today Proceed 52 (2022) 2201–2204, https://doi.org/10.1016/j.matpr.2021.07.315.
[41] T.N. Babu, D. Patel, D. Tharnari, A. Bhatt, Temperature behavior-based monitoring of worm gears under different working conditions, in: Innov. Des. Anal. Dev. Pract. Aerosp. Automot. Eng., 2, Springer Singapore, 2019, pp. 257–265, https://doi.org/10.1007/978-981-13-2718-6_24.
[42] Y. Shi, Y. Yao, J. Fei, Analysis of bulk temperature field and flash temperature for locomotive traction gear, Appl. Therm. Eng. 99 (2016) 528–536, https://doi.org/10.1016/j.applthermaleng.2016.01.093.
[43] W. Li, P. Zhai, L. Ding, Analysis of thermal characteristic of spur/helical gear transmission, J. Therm. Sci. Eng. Appl. 11 (2) (2019) 021003, https://doi.org/10.1115/1.4041597.
[44] W. Li, J. Tian, Unsteady-state temperature field and sensitivity analysis of gear transmission, Tribol. Int. 116 (2017) 229–243, https://doi.org/10.1016/j.triboint.2017.07.019.
[45] W. Li, D. Pang, W. Hao, Effects of the helix angle, the friction coefficient and mechanical errors on unsteady-state temperature field of helical gear and thermal sensitivity analysis, Int. J. Heat. Mass Transf. 144 (2019) 118669, https://doi.org/10.1016/j.ijheatmasstransfer.2019.118669.
[46] W. Li, P. Zhai, J. Tian, B. Luo, Thermal analysis of helical gear transmission system considering machining and installation error, Int. J. Mech. Sci. 149 (2018) 1–17, https://doi.org/10.1016/j.ijmecsci.2018.09.036.
[47] F. Lu, M. Wang, W. Liu, H. Bao, R. Zhu, CFD-based calculation method of convective heat transfer coefficient of spiral bevel gear in intermediate gearbox under splash lubrication, Ind. Lubri. Tribol. 73 (3) (2021) 470–476, https://doi.org/10.1108/ILT-07-2020-0233.
[48] F. Lu, M. Wang, W. Pan, H. Bao, W. Ge, CFD-based investigation of lubrication and temperature characteristics of an intermediate gearbox with splash lubrication, Appl. Sci. 11 (2021) 352, https://doi.org/10.3390/app11010352.
[49] N. Basha, A. Kovacevic, S. Rane, Numerical investigation of oil injection in screw compressors, Appl. Therm. Eng. 193 (2021) 116959, https://doi.org/10.1016/j.applthermaleng.2021.116959.
[50] J.D. de Gevigney, C. Changenet, F. Ville, P. Velex, Thermal modelling of a back-to-back gearbox test machine: application to the FZG test rig, Proc. Inst. Mech. Eng. Part J: J. Eng. Tribol. 226((6) (2012) 501–515, https://doi.org/10.1177/1350650111433243.
[51] A. Monot, T. Touret, C. Changenet, F. Ville, T. Grandgeorge, F. Fayolle, A method to develop a high-fidelity gearbox thermal model based on limited temperature measurements, Mech. Base. Des. Struct. Mach. (2024) 1–21, https://doi.org/10.1080/15397734.2024.2383962.
[52] X. Ning, M. Chen, Z. Zhou, Y. Shu, W. Xiong, Y. Cao, X. Shang, Z. Wang, Thermal analysis of automobile drive axles by the thermal network method, World Electr. Veh. J. 13 (2022) 75, https://doi.org/10.3390/wevj13050075.
[53] C. Changenet, X. Oviedo-Marlot, P. Velex, Power loss predictions in geared transmissions using thermal networks-applications to a six-speed manual gearbox, J. Mech. Des. 128 (3) (2006) 618–625, https://doi.org/10.1115/1.2181601.
[54] L. Chen, X. Wu, D. Qin, Z. Wen, Thermal network model for temperature prediction in planetary gear trains, Appl. Mech. Mater. 86 (2011) 415–418, https://doi.org/10.4028/www.scientific.net/AMM.86.415.
[55] X. Deng, S. Wang, Y. Hammi, L. Qian, Y. Liu, A combined experimental and computational study of lubrication mechanism of high precision reducer adopting a worm gear drive with complicated space surface contact, Tribol. Int. 146 (2020) 106261, https://doi.org/10.1016/j.triboint.2020.106261.
[56] S. Koshizuka, Y. Oka, Moving-particle semi-implicit method for fragmentation of incompressible fluid, Nucl. Sci. Eng. 123 (3) (1996) 421–434, https://doi.org/10.13182/NSE96-A24205.
[57] C. Wei, W. Wu, X. Hou, D. Nelias, S. Yuan, Research on flow pattern of low temperature lubrication flow field of rotating disk based on MPS method, Tribol. Int. 180 (2023) 108221, https://doi.org/10.1016/j.triboint.2023.108221.
[58] C.M.C.G. Fernandes, D.M.P. Rocha, R.C. Martins, L. Magalhães, J.H.O. Seabra, Finite element method model to predict bulk and flash temperatures on polymer gears, Tribol. Int. 120 (2018) 255–268, https://doi.org/10.1016/j.triboint.2017.12.027.
[59] S. Seetharaman, A. Kahraman, Load-independent spin power losses of a spur gear pair: model formulation, J. Tribol. 131 (2) (2009) 022201, https://doi.org/10.1115/1.3085943.
[60] H. Long, A.A. Lord, D.T. Gethin, B.J. Roylance, Operating temperatures of oil-lubricated medium-speed gears: numerical models and experimental results, Proc. Inst. Mech. EnG. Part G. J. Aero. EnG. 217 (2) (2003) 87–106, https://doi.org/10.1243/095441003765208745.
[61] S. Shao, K. Zhang, Y. Yao, Y. Liu, J. Gu, Investigations on lubrication characteristics of high-speed electric multiple unit gearbox by oil volume adjusting device, J. Zhejiang Univ. Sci. A 23 (12) (2022) 1013–1026, https://doi.org/10.1631/jzus.A2200274.
[62] E.C. Cobb, O.A. Saunders, Heat transfer from a rotating disk, Proc. R. Soc. Lond. 236 (1956) 343–351, https://doi.org/10.1098/rspa.1956.0141.

[63] C. Wanger, Heat transfer from a rotating disk to ambient air, J. Appl. Phys. 19 (1948) 837–839, https://doi.org/10.1063/1.1698216.
[64] M. Siddique, M. Alhazmy, Experimental study of turbulent single-phase flow and heat transfer inside a micro-finned tube, Int. J. Refrig 31 (2008) 234–241, https://doi.org/10.1016/j.ijrefrig.2007.06.005.
[65] C. Paschold, M. Sedlmair, T. Lohner, K. Stahl, Calculating component temperatures in gearboxes for transient operation conditions, Forch. Ing. 86 (2022) 521–534, https://doi.org/10.1007/s10010-021-00532-4.
[66] C. Paschold, M. Sedlmair, T. Lohner, K. Stahl, Efficiency and heat balance calculation of worm gears, Forch. Ing. 84 (2020) 115–125, https://doi.org/10.1007/s10010-019-00390-1.
[67] Prometech Software, Particle Works Theory Manual, Prometech Software, Inc, 2016.
[68] W. Ding, S. Yan, W. Miao, L. Zhou, Z. Liu, Study on thermal balance analysis technology of rail traffic gearbox, J. Mech. Transm. 45 (5) (2021) 96–100, https://doi.org/10.16578/i.issn.1004.2539.2021.05.014.
[69] T.A. Harris. Rolling Bearing Analysis, 4th. Edition, Wiley-Interscience, 2000.
[70] TB/T 3134–2023, Driving gearbox of rolling stock - General requirement, (2024) TB/T 3134–2023.
[71] H.P. Otto, Flank load carrying capacity and power loss reduction by minimised lubrication [PhD thesis], Technical University of Munich, 2009.
[72] M. Yazdani, M.C. Soteriou, F. Sun, Z. Chaudhry, Prediction of the thermo-fluids of gearbox systems, Int. J. Heat. Mass Tran 81 (2015) 337–346, https://doi.org/10.1016/j.ijheatmasstransfer.2014.10.038.